The Dishevelled-binding protein CXXC5 negatively regulates cutaneous wound healing

Soung-Hoon Lee,[1,2] Mi-Yeon Kim,[1,2] Hyun-Yi Kim,[1,2] Young-Mi Lee,[1,2] Heesu Kim,[3] Kyoung Ae Nam,[3] Mi Ryung Roh,[3] Do Sik Min,[1,4] Kee Yang Chung,[3] and Kang-Yell Choi[1,2]

[1]Translational Research Center for Protein Function Control; [2]Department of Biotechnology, College of Life Science and Biotechnology; and [3]Department of Dermatology, Severance Hospital, Cutaneous Biology Research Institute, College of Medicine; Yonsei University, Seoul 120-749, South Korea
[4]Department of Molecular Biology, College of Natural Science, Pusan National University, Busan 609-735, South Korea

Wnt/β–catenin signaling plays important roles in cutaneous wound healing and dermal fibrosis. However, its regulatory mechanism has not been fully elucidated, and a commercially available wound–healing agent targeting this pathway is desirable but currently unavailable. We found that CXXC-type zinc finger protein 5 (CXXC5) serves as a negative feedback regulator of the Wnt/β–catenin pathway by interacting with the Dishevelled (Dvl) protein. In humans, CXXC5 protein levels were reduced in epidermal keratinocytes and dermal fibroblasts of acute wounds. A differential regulation of β–catenin, α–smooth muscle actin (α–SMA), and collagen I by overexpression and silencing of CXXC5 in vitro indicated a critical role for this factor in myofibroblast differentiation and collagen production. In addition, CXXC5−/− mice exhibited accelerated cutaneous wound healing, as well as enhanced keratin 14 and collagen synthesis. Protein transduction domain (PTD)–Dvl-binding motif (DBM), a competitor peptide blocking CXXC5-Dvl interactions, disrupted this negative feedback loop and activated β–catenin and collagen production in vitro. Co-treatment of skin wounds with PTD–DBM and valproic acid (VPA), a glycogen synthase kinase 3β (GSK3β) inhibitor which activates the Wnt/β–catenin pathway, synergistically accelerated cutaneous wound healing in mice. Together, these data suggest that CXXC5 would represent a potential target for future therapies aimed at improving wound healing.

CORRESPONDENCE
Kang-Yell Choi:
kychoi@yonsei.ac.kr

Abbreviations used: α-SMA, α-smooth muscle actin; DBM, Dvl-binding motif; Dkk-1, Dickkopf-1; Dvl, Dishevelled; ECM, extracellular matrix; EGF, epidermal growth factor; GSK3β, glycogen synthase kinase 3β; ICC, immunocyto-chemical; IHC, immunohisto-chemistry; PCNA, proliferating cell nuclear antigen; PFA, para-formaldehyde; PTD, protein transduction domain; SFRP1, secreted frizzled-related protein 1; VPA, valproic acid; WCL, whole cell lysate.

Cutaneous wound healing is a dynamic and interactive process involving endothelial cells, blood cells, epidermal keratinocytes, and dermal fibroblasts (Singer and Clark, 1999; Yamaguchi and Yoshikawa, 2001). The dermal fibroblasts are the cells responsible for extracellular matrix (ECM) and collagen deposition (Singer and Clark, 1999; Diegelmann and Evans, 2004). Normal cutaneous wound healing requires fibroblast proliferation and migration into the wound bed, followed by tightly regulated ECM deposition and contraction (Chipev and Simon, 2002). Aberrant regulation of these processes occurs in fibrotic diseases such as keloid formation, morphea, and scleroderma (Krieg et al., 1985; Kähäri et al., 1988; Ladin et al., 1995). Understanding the mechanisms that regulate cutaneous wound healing and collagen production is necessary to develop better therapies for the treatment of acute and chronic wounds (Guo and Dipietro, 2010).

The Wnt/β-catenin pathway, which is also called the canonical Wnt pathway (Barker, 2008), plays important roles in cutaneous wound healing and dermal fibrosis (Zhang et al., 2009a; Wei et al., 2011). Levels of β-catenin protein are elevated during the proliferative phase of cutaneous wound healing (Labus et al., 1998; Cheon et al., 2005). The Wnt/β-catenin pathway is also aberrantly activated in certain human fibrotic diseases, which are characterized by increased nuclear accumulation of β-catenin (Sato, 2006; Akhmetshina et al., 2012). The activation of the Wnt/β-catenin pathway involves dermal fibrosis and myofibroblast differentiation through up-regulation of TGF-β pathways (Carthy et al., 2011; Wei et al., 2011; Akhmetshina

The Rockefeller University Press $30.00
J. Exp. Med. 2015 Vol. 212 No. 7   1061–1080
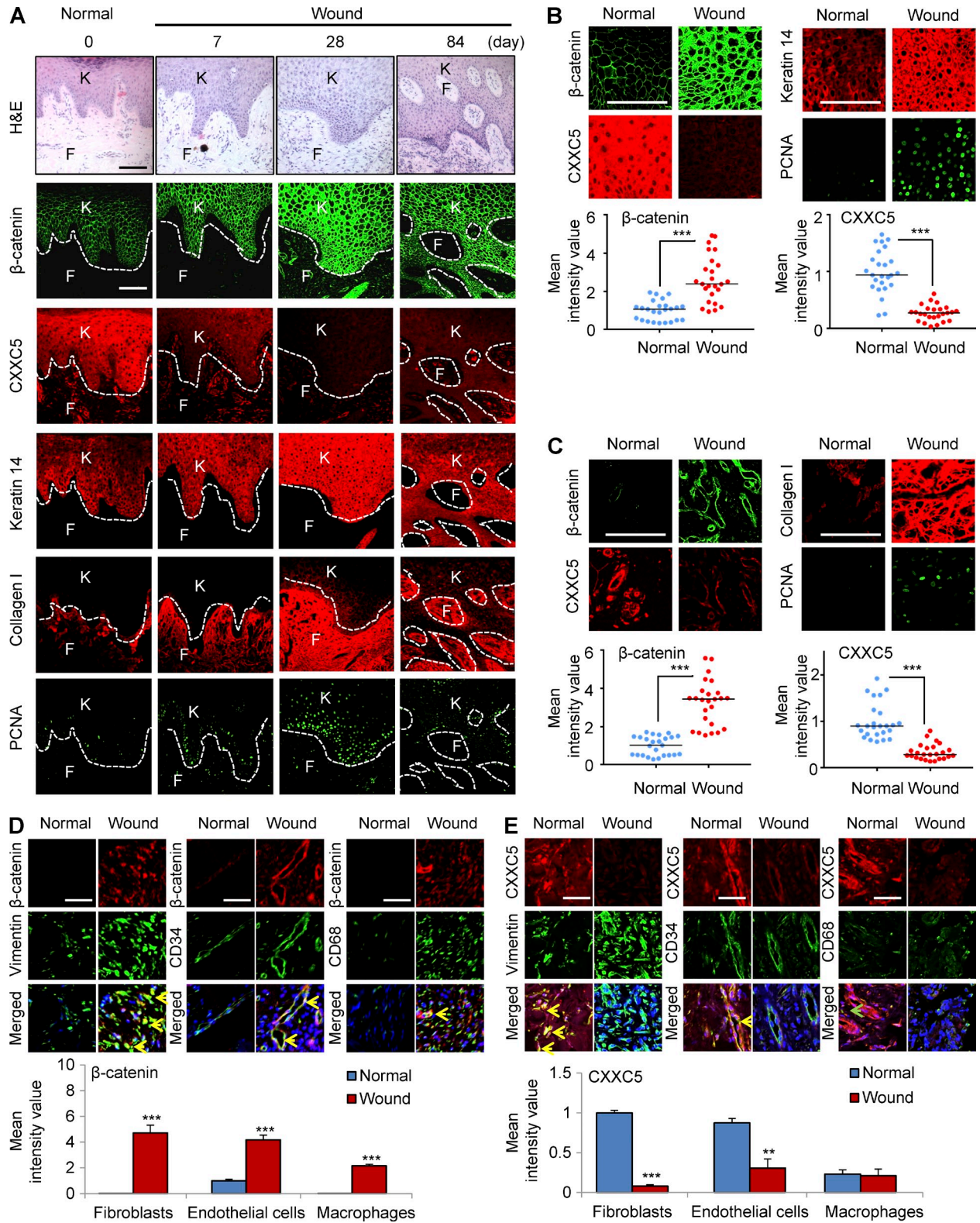www.jem.org/cgi/doi/10.1084/jem.20141601

1061

Figure 1.   CXXC5 levels are inversely associated with the levels of β-catenin and wound-healing markers in human acute wounds. Wounded tissues (*n* = 5 samples) were excised from wound margins at 0, 7, 28, and 84 d after surgery in melanoma patients and subjected to H&E staining and immunohistochemical analyses. 0 d represents normal healthy biopsy (control). (A) Representative H&E and confocal (IHC) images (*n* = 5 independent experiments) for β-catenin, CXXC5, keratin 14, collagen I, or PCNA in the wounds are shown. Dashed lines indicate the epidermal–dermal boundary. F, fibroblasts; K, keratinocytes. (B and C, top) High magnification of representative IHC images for β-catenin, CXXC5, and the indicated wound-healing

et al., 2012). Inactivation of glycogen synthase kinase 3β (GSK3β), a multifunctional serine/threonine kinase which phosphorylates and destabilizes β-catenin (Doble and Woodgett, 2003), also plays an important role in the wound-healing process (Bergmann et al., 2011). GSK3β in dermal fibroblasts controls wound healing and fibrosis through a β-catenin–dependent mechanism (Bergmann et al., 2011). GSK3β inhibitors, such as valproic acid (VPA) or SB216763, induce cutaneous wound healing and dermal fibrosis by activation of the Wnt/β-catenin pathway (Bergmann et al., 2011; Lee et al., 2012).

CXXC5 is a newly identified CXXC-type zinc finger family protein (Zhang et al., 2009b) that negatively regulates the Wnt/β-catenin pathway as a Wilms Tumor 1 (WT1) transcriptional target (Andersson et al., 2009; Kim et al., 2010a). CXXC5 contains a C-terminal Dishevelled (Dvl)-binding domain, which facilitates interaction with Dvl. This domain was previously identified in Idax (Hino et al., 2001) and is essential for CXXC5 function as a negative regulator of the Wnt/β-catenin pathway (London et al., 2004; Kim et al., 2010a). Furthermore, CXXC5 is important for neogenesis in the zebrafish (Kim et al., 2010a). CXXC5 also acts as a BMP4-induced inhibitor of the Wnt/β-catenin pathway in neural stem cells (Andersson et al., 2009). Although the role of CXXC5 in the regulation of the Wnt/β-catenin pathway has been demonstrated, the effect of CXXC5 on cutaneous wound healing and collagen production has yet to be illustrated. In this study, we investigated the status of CXXC5 during the wound-healing process in human melanoma patients and characterized the effect of CXXC5 on wound healing and collagen production in vitro and in vivo.

RESULTS
CXXC5 levels are decreased in acute wounds in humans
To identify the involvement of CXXC5 in cutaneous wound healing in a human model, we investigated the status of CXXC5 in surgical wounds after the removal of melanomas. We monitored levels of β-catenin, CXXC5, and wound-healing markers during the healing process for up to 3 mo in five acute wound tissue specimens from patients using immunohistochemical analyses. Protein levels of β-catenin gradually increased and peaked 28 d after the operation (Fig. 1 A). The expression of keratin 14, collagen I, and proliferating cell nuclear antigen (PCNA) correlated directly with that of β-catenin during wound healing (Fig. 1 A). CXXC5 expression was reduced in surgical wounds; its expression patterns were opposite of those of β-catenin in the same wounded tissue area

(Fig. 1 A). We also confirmed the expression of β-catenin and wound-healing markers in epidermal keratinocytes and dermal fibroblasts, respectively. The levels of β-catenin, keratin 14, and PCNA in keratinocytes were increased in wounds compared with normal skin (Fig. 1 B). Conversely, CXXC5 expression was decreased in the keratinocytes from wounded tissues (Fig. 1 B). The concurrent increases in β-catenin, collagen I, and PCNA in fibroblasts of wound tissue were also observed in the magnified images (Fig. 1 C). In contrast, CXXC5 expression was reduced in fibroblasts of wound tissues (Fig. 1 C). Quantitative TissueFAXS analysis of immunohistochemical staining also confirmed the inverse expression patterns of β-catenin and CXXC5 in wound tissues (Fig. 1, B and C). For comprehensive analysis of β-catenin and CXXC5 expression in human skin tissues, we performed co-immunostaining with those proteins and markers for fibroblasts (vimentin), endothelial cells (CD34), and macrophages (CD68). β-Catenin was primarily expressed in endothelial cells of normal skin, and its level was significantly increased in fibroblasts, endothelial cells, or macrophages in the dermis of wounds (Fig. 1 D). CXXC5 was mainly expressed in fibroblasts or endothelial cells in the dermis of human normal skin, and its level was significantly decreased in fibroblasts in the dermis of human wounds (Fig. 1 E). Overall, these data show an inverse relationship between CXXC5 protein expression and active Wnt/β-catenin signaling in wound tissues.

CXXC5 inhibits collagen production in vitro
CXXC5 is known as a negative regulator of the Wnt/β-catenin pathway (Kim et al., 2010a). Considering the relationship between the Wnt/β-catenin pathway and fibrosis (Wei et al., 2011; Akhmetshina et al., 2012), we examined the effect of *CXXC5* transfection on myofibroblast differentiation and collagen production in human dermal fibroblasts. Transfection with *CXXC5* markedly inhibited β-catenin expression in a dose-dependent manner (Fig. 2 A). The levels of α-smooth muscle actin (α-SMA) and collagen I were diminished by *CXXC5* transfection (Fig. 2 A). Expression of endothelin-1, a target of the Wnt/β-catenin pathway (Kim et al., 2005; Chen et al., 2007) and a marker for collagen production (Rizvi et al., 1996), was also significantly decreased after *CXXC5* transfection (Fig. 2 A). To further characterize the role of CXXC5 in myofibroblast differentiation and collagen production, we examined the effect of CXXC5 knockdown on myofibroblast differentiation and collagen production. Expressions of β-catenin, α-SMA, collagen I, and endothelin-1 were increased by siRNA-mediated CXXC5 knockdown (Fig. 2 B).

markers in keratinocytes (B) and fibroblasts (C) are shown. (bottom) Quantitative TissueFAXS analyses of IHC staining for β-catenin and CXXC5 (*n* = 5 independent experiments) were performed in five random, representative fields per each patient sample. Horizontal lines represent the mean fluorescence intensities. Student's *t* test was used (***, P < 0.0005). (D and E, top) Representative images of IHC staining performed with antibodies against β-catenin (D) or CXXC5 (E) and markers for fibroblasts (vimentin), endothelial cells (CD34), or macrophages (CD68). Yellow arrowheads indicate the co-expression of β-catenin or CXXC5 and markers for fibroblasts, endothelial cells, or macrophages, and the green arrowhead indicates the cells expressing only CD68. (bottom) Quantitative TissueFAXS analyses of IHC staining for β-catenin and CXXC5 (*n* = 3 independent experiments) were performed in three random, representative fields (**, P < 0.005; ***, P < 0.0005). Means ± SD. Bars: (A–C) 100 µm; (D and E) 50 µm.
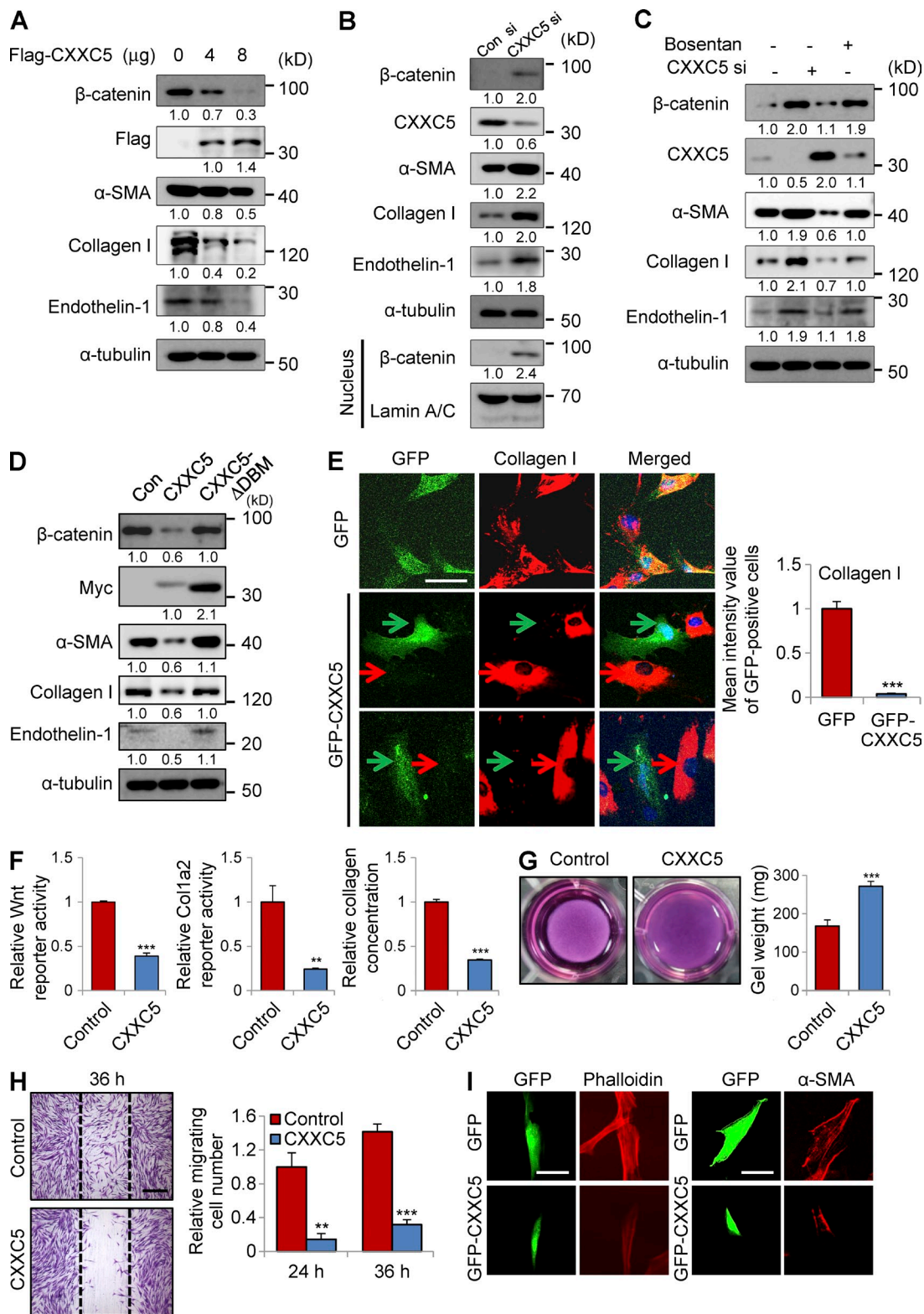
Figure 2. CXXC5 attenuates myofibroblast differentiation and collagen production in human dermal fibroblasts. (A–D) Human dermal fibroblasts (n = 2–3 cells) were transfected with pcDNA3.0-CXXC5-Flag (A) at the indicated concentration, 100 nM CXXC5 siRNA (B and C), and pcDNA3.1-CXXC5-Myc and pcDNA3.1-CXXC5ΔDBM-Myc (D), together with corresponding control plasmid (Con) or control siRNA (Con si). The cells transfected with CXXC5 siRNA (C) or control siRNA were treated with or without 10 µM bosentan. The cells were further cultured for 2 d and harvested, and whole cell lysates (WCLs) were subjected to Western blot analyses to detect the protein levels of β-catenin, endothelin-1, α-SMA, and collagen I (n = 2 independent

Moreover, CXXC5 knockdown induced β-catenin nuclear translocation as shown by cell fractionation and Western blotting (Fig. 2 B). Collagen production induced by CXXC5 knockdown was abolished by bosentan, a dual endothelin receptor antagonist, indicating that CXXC5 knockdown induced collagen production through an endothelin-1–dependent mechanism (Fig. 2 C). CXXC5 contains a C-terminal Dvl-binding motif (DBM) that is essential for CXXC5 function as a negative regulator of the Wnt/β-catenin pathway (London et al., 2004). Inhibition of β-catenin expression, as well as reduced expressions of α-SMA, collagen I, and endothelin-1, was abolished when CXXC5ΔDBM, a CXXC5 mutant with a DBM deletion (London et al., 2004), was expressed (Fig. 2 D). Immunocytochemical (ICC) analysis showed that collagen I expression was specifically abolished in *GFP-CXXC5*–transfected cells (Fig. 2 E). The Wnt/β-catenin reporter activity, *Col1a2* promoter activity, and the level of collagen in the supernatant were significantly lowered by CXXC5 overexpression (Fig. 2 F). Moreover, overexpression of CXXC5 inhibited the ability of fibroblasts to contract collagen gels (Fig. 2 G), cell motility (Fig. 2 H), and the formation of stress fibers (Fig. 2 I).

CXXC5 is a negative feedback regulator of the Wnt/β-catenin pathway functioning via Wnt3a–dependent Dvl interaction

To confirm the role of the Wnt/β-catenin pathway in CXXC5 function, we examined the effect of Wnt3a in human dermal fibroblasts. Wnt3a treatment induced expressions of β-catenin, α-SMA, and collagen I (Fig. 3 A). Interestingly, both mRNA and protein levels of CXXC5 were increased by treatment with Wnt3a (Fig. 3 A). ICC analysis also showed that Wnt3a increased expression of CXXC5, in concert with that of β-catenin and collagen I, in a dose-dependent manner (Fig. 3 B). Both β-catenin and CXXC5 were concomitantly increased in a time-dependent manner by Wnt3a treatment, and maximal levels were reached at 48 h (Fig. 3 C). Considering the role of CXXC5 as a negative regulator of the Wnt/β-catenin pathway, we hypothesized that Wnt3a–dependent induction of CXXC5 may be the negative feedback mechanism. This notion was further indicated by synergistic increases in the expression of β-catenin, α-SMA, and collagen I by co-treatment with CXXC5

siRNA and Wnt3a (Fig. 3 D). Both β-catenin and CXXC5 were also increased in the nucleus and cytosol, respectively, by Wnt3a treatment, and β-catenin levels were synergistically increased by co-treatment with CXXC5 siRNA and Wnt3a, as shown by ICC analysis (Fig. 3 E). To further characterize the role of CXXC5 as a negative feedback regulator that functions via Dvl-1, we assessed the interaction of wild-type CXXC5 or its deletion mutant CXXC5 ΔDBM with Dvl-1. CXXC5, but not CXXC5 ΔDBM, interacted with Dvl-1, and this interaction was enhanced by Wnt3a treatment (Fig. 3 F). Consistently, Wnt3a-induced increase in β-catenin was significantly reduced by overexpression of CXXC5 but not of CXXC5 ΔDBM. We also observed an enhanced interaction between CXXC5 and Dvl-1 by Wnt3a in the endogenous level (Fig. 3 G). Overall, CXXC5 is a negative feedback regulator of the Wnt/β-catenin pathway in human dermal fibroblasts and functions via binding to Dvl in a manner dependent on Wnt3a.

CXXC5−/− mice show accelerated cutaneous wound healing and enhanced keratin 14 and collagen I synthesis

To identify a role for CXXC5 in cutaneous wound healing and collagen production in vivo, we used *CXXC5*−/− mice, which were generated by inactivating exon 2 of *CXXC5* (Kim et al., 2014a). We created full-thickness wounds (diameter = 1.5 cm) on the backs of *CXXC5*+/+ and *CXXC5*−/− mice and then monitored expression of wound–healing markers. The sizes of wounds in *CXXC5*−/− mice were markedly reduced compared with those of wounds in *CXXC5*+/+ mice (Fig. 4 A). Histological analysis also showed that the distance between the wound edges was decreased in *CXXC5*−/− mice compared with that in *CXXC5*+/+ mice (Fig. 4 B). We also found that *CXXC5*−/− mice showed a marked acceleration in wound closure compared with *CXXC5*+/+ mice, as determined by measurement of wound diameters (Fig. 4 C). The rate of wound closure in *CXXC5*−/− mice was accelerated by 16 to approximately 32% compared with that in *CXXC5*+/+ mice during the proliferative phase of wound healing. The levels of collagen deposition were increased in *CXXC5*−/− mice, as detected by stainings with Masson's trichrome, picrosirius red, and van Gieson (Fig. 4 D). Expression of keratin 14, collagen I, and PCNA was increased in conjunction with β-catenin

experiments). Relative densitometric ratios of each protein to loading control (α-tubulin or lamin A/C) are shown. (E) Human dermal fibroblasts were transfected with pEGFP-c3 or GFP-CXXC5 and further cultured for 2 d. The cells were immunocytochemically stained for collagen I. Representative confocal (ICC) images are shown (left), and mean intensity quantitation in GFP-positive cells was performed (right; ***, P < 0.0005; *n* = 3 independent experiments). Red arrows indicate the expression of collagen I, and green arrows indicate the expression of GFP. (F) Wnt luciferase reporter activity (left), *Col1a2* luciferase reporter activity (middle), and collagen concentration (right) in the supernatant of human dermal fibroblasts were measured after transfection with pcDNA3.0 or pcDNA3.0-CXXC5-Flag (*n* = 3 independent experiments). Values are presented relative to control (**, P < 0.005; ***, P < 0.0005). (G) Contraction of collagen gels was monitored by measuring gel weight after transfection with pcDNA3.0-CXXC5-Flag (*n* = 3 independent experiments). Representative images (left) and quantitation (right) are shown (***, P < 0.0005). (H) The cells transfected with pcDNA3.0 or pcDNA3.0-CXXC5-Flag were scratched with sterile pipette tips and incubated in medium containing 5% serum for 36 h. Cells were then fixed with 4% PFA and stained with crystal violet. Representative microscopy images are shown (left), and cell migration was measured by counting migrating cells (right; **, P < 0.005; ***, P < 0.0005; *n* = 3 independent experiments). Dashed lines represent the widths of the initially scratched wounds. (I) ICC staining of human dermal fibroblasts transfected with GFP or GFP-CXXC5 was performed to detect phalloidin (left) and α-SMA (right). Representative ICC images are shown (*n* = 3 independent experiments). Means ± SD. Bars: (E and I) 50 μm; (H) 500 μm.
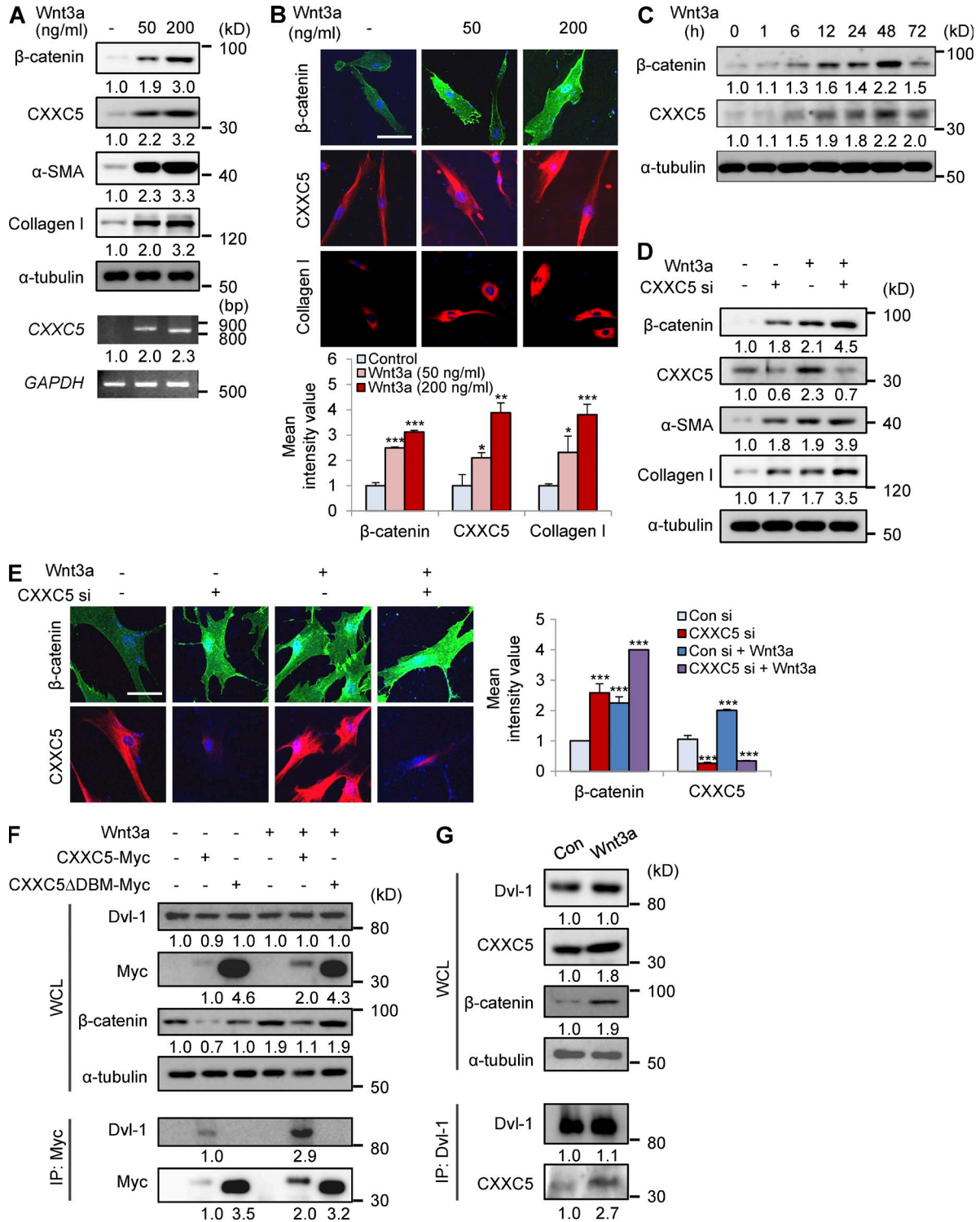
Figure 3. Wnt3a induces CXXC5 expression and enhances CXXC5–Dvl interaction. (A and B) Human dermal fibroblasts (n = 2–3 cells) were treated with or without Wnt3a (50 or 200 ng/ml). (A) WCLs were subjected to Western blot analyses with antibodies against β-catenin, CXXC5, α-SMA, collagen I, or α-tubulin and to RT-PCR analyses with primers for *CXXC5* or *GAPDH* (n = 2 independent experiments). (B) Relative densitometry values are shown underneath blots as ratios relative to the levels of loading control (α-tubulin or *GAPDH*). The cells were also immunocytochemically stained for β-catenin, CXXC5, or collagen I. Representative ICC images are shown (top), and mean intensity quantitation was performed (bottom; *, P < 0.05; **, P < 0.005; ***, P < 0.0005; n = 3 independent experiments). (C) Human dermal fibroblasts were incubated with 50 ng/ml Wnt3a for 1, 6, 12, 24, 48, or 72 h, and WCLs were subjected to Western blot analyses with antibodies against β-catenin, CXXC5, or α-tubulin (n = 2 independent experiments). Relative densitometric ratios of each protein to α-tubulin are shown. (D and E) Human dermal fibroblasts were treated with 50 ng/ml Wnt3a for 2 d after treatment

expression in *CXXC5*$^{-/-}$ mice (Fig. 4 D). Quantitative analysis of collagen synthesis using a hydroxyproline assay showed enhanced collagen production after 12 d in wound tissues of *CXXC5*$^{-/-}$ mice compared with those of *CXXC5*$^{+/+}$ mice (Fig. 4 E). In wounded skin sections, quantitative immunofluorescence TissueFAXS analyses revealed a more than fourfold increase in β-catenin protein levels in both keratinocytes and fibroblasts of *CXXC5*$^{-/-}$ mice compared with those in wild-type mice (Fig. 4 F). Keratin 14 levels in keratinocytes were increased 2.4-fold, and collagen I levels in fibroblasts were increased 6.3-fold in *CXXC5*$^{-/-}$ mice compared with wild-type mice (Fig. 4 F). To analyze the expression of Wnt/β-catenin pathway target genes, mRNA levels of *c-Myc*, *cyclin D1*, and *endothelin-1* were monitored by RT-PCR analysis of wound tissues in *CXXC5*$^{+/+}$ and *CXXC5*$^{-/-}$ mice. Expression levels of *c-Myc* and *cyclin D1*, markers of oncogenesis (Liao et al., 2007), were not significantly changed in wounds of *CXXC5*$^{-/-}$ mice as compared with wild-type mice, but expression of *endothelin-1*, a marker of collagen production (Rizvi et al., 1996), was significantly increased in the *CXXC5*$^{-/-}$ mice (Fig. 4 G). Moreover, endothelin-1 was specifically increased in fibroblasts of *CXXC5*$^{-/-}$ mice, as revealed by immunohistochemical analysis (Fig. 4 H). Therefore, CXXC5 specifically regulates Wnt/β-catenin signaling target genes involved in stimulation of wound healing without changing expression of genes involved in oncogenic transformation of cells.

Endothelin receptor antagonists reversed the accelerated wound–healing phenotype of *CXXC5*$^{-/-}$ mice

Endothelin-1 is a direct target of the Wnt/β-catenin pathway in NIH3T3 fibroblasts (Chen et al., 2007) and is associated with wound healing and fibrosis (Rizvi et al., 1996). To investigate whether the accelerated wound-healing phenotype in *CXXC5*$^{-/-}$ mice was dependent on endothelin-1, *CXXC5*$^{+/+}$ and *CXXC5*$^{-/-}$ mice were fed bosentan on a daily basis for 11 d. Bosentan reversed the accelerated wound-healing phenotype observed in *CXXC5*$^{-/-}$ mice and decreased levels of β-catenin, keratin 14, collagen I, and PCNA (Fig. 5, A and B). Western blot analyses also showed that bosentan reduced β-catenin and wound-healing markers in *CXXC5*$^{-/-}$ mice through an endothelin-1–dependent mechanism (Fig. 5 C). Bosentan also decreased collagen deposition in *CXXC5*$^{-/-}$ mice, as determined by Masson's trichrome, picrosirius red, and van Gieson staining and hydroxyproline analyses (Fig. 5, D and E). Quantitative

TissueFAXS analyses also showed that induction of β-catenin and wound-healing markers (keratin 14 and collagen I) in keratinocytes and fibroblasts of *CXXC5*$^{-/-}$ mouse wounds was reversed by bosentan (Fig. 5 F).

VPA treatment further accelerated cutaneous wound healing and synergistically enhanced keratin 14 and collagen I synthesis in *CXXC5*$^{-/-}$ mice

To confirm that CXXC5 functioned as a negative feedback regulator of the Wnt/β-catenin pathway in vivo, we treated the wounds of *CXXC5*$^{+/+}$ and *CXXC5*$^{-/-}$ mice with VPA, a Wnt/β-catenin pathway activator (Gould and Manji, 2002; Gould et al., 2004). Interestingly, *CXXC5*$^{-/-}$ mice treated with VPA displayed markedly accelerated wound healing (Fig. 6, A and B). Moreover, expression levels of β-catenin, keratin 14, collagen I, α-SMA, and PCNA were synergistically increased in VPA-treated *CXXC5*$^{-/-}$ mice, as determined by immunohistochemical and Western blot analyses (Fig. 6, A and C); however, VPA-treated *CXXC5*$^{-/-}$ mice did not show significant changes in expression of c-Myc and cyclin D1 (Fig. 6 C). Stainings with Masson's trichrome, picrosirius red, and van Gieson in combination with results of the hydroxyproline assay also confirmed that collagen expression was synergistically increased in VPA-treated *CXXC5*$^{-/-}$ mice (Fig. 6, D and E). Quantitative TissueFAXS analyses also showed that β-catenin and wound-healing markers were significantly increased in keratinocytes and fibroblasts of VPA-treated *CXXC5*$^{-/-}$ mouse wounds (Fig. 6 F). Overall, blockade of CXXC5 function in concert with activation of the Wnt/β-catenin pathway is a potential approach for the development of drugs to enhance wound healing.

Protein transduction domain (PTD)–DBM induces expression of β–catenin, α–SMA, and collagen I

To activate the Wnt/β-catenin pathway by disrupting the negative feedback regulation of CXXC5, we used competitor peptides that interfere with the CXXC5-Dvl interaction. These synthetic peptides were composed of a PTD for delivery (Matsushita and Matsui, 2005), a linker for flexibility, DBM, and lysine conjugated with FITC for visualization (Fig. 7 A). The PTD-DBM peptide induced the expression of β-catenin, α-SMA, and collagen I in a concentration–dependent manner in human dermal fibroblasts (Fig. 7 B). PTD-DBM specifically increased both mRNA and protein levels of endothelin-1 but

with control siRNA (Con si) or CXXC5 siRNA (CXXC5 si). (D) Western blot analysis (*n* = 3 independent experiments) of WCLs was performed with antibodies against β-catenin, α-SMA, collagen I, CXXC5, or α-tubulin. Relative densitometry values are shown underneath the blots as ratios relative to the levels of α-tubulin. ICC analysis (*n* = 3 independent experiments) of samples in D and E was performed with β-catenin or CXXC5. (E) Representative ICC images are shown (left), and mean intensity values were calculated (right; ***, P < 0.0005). (B and E) Bars, 50 μm. Means ± SD. (F) Human dermal fibroblasts were transfected with pcDNA3.1, pcDNA3.1-CXXC5-Myc, or pcDNA3.1-CXXC5ΔDBM-Myc. WCLs or cell lysates immunoprecipitated with anti-Myc were analyzed by immunoblotting to detect Dvl-1, Myc, β-catenin, or α-tubulin (*n* = 2 independent experiments). Relative densitometry values are shown below the blots. (G) WCLs from human dermal fibroblasts treated with (Wnt3a) or without (Con) 50 ng/ml Wnt3a for 2 d were subjected to immunoprecipitation with anti–Dvl-1 antibody, and Western blot analyses were subsequently performed to detect Dvl-1, CXXC5, β-catenin, and α-tubulin (*n* = 2 independent experiments). Relative densitometry values are shown below the blots.
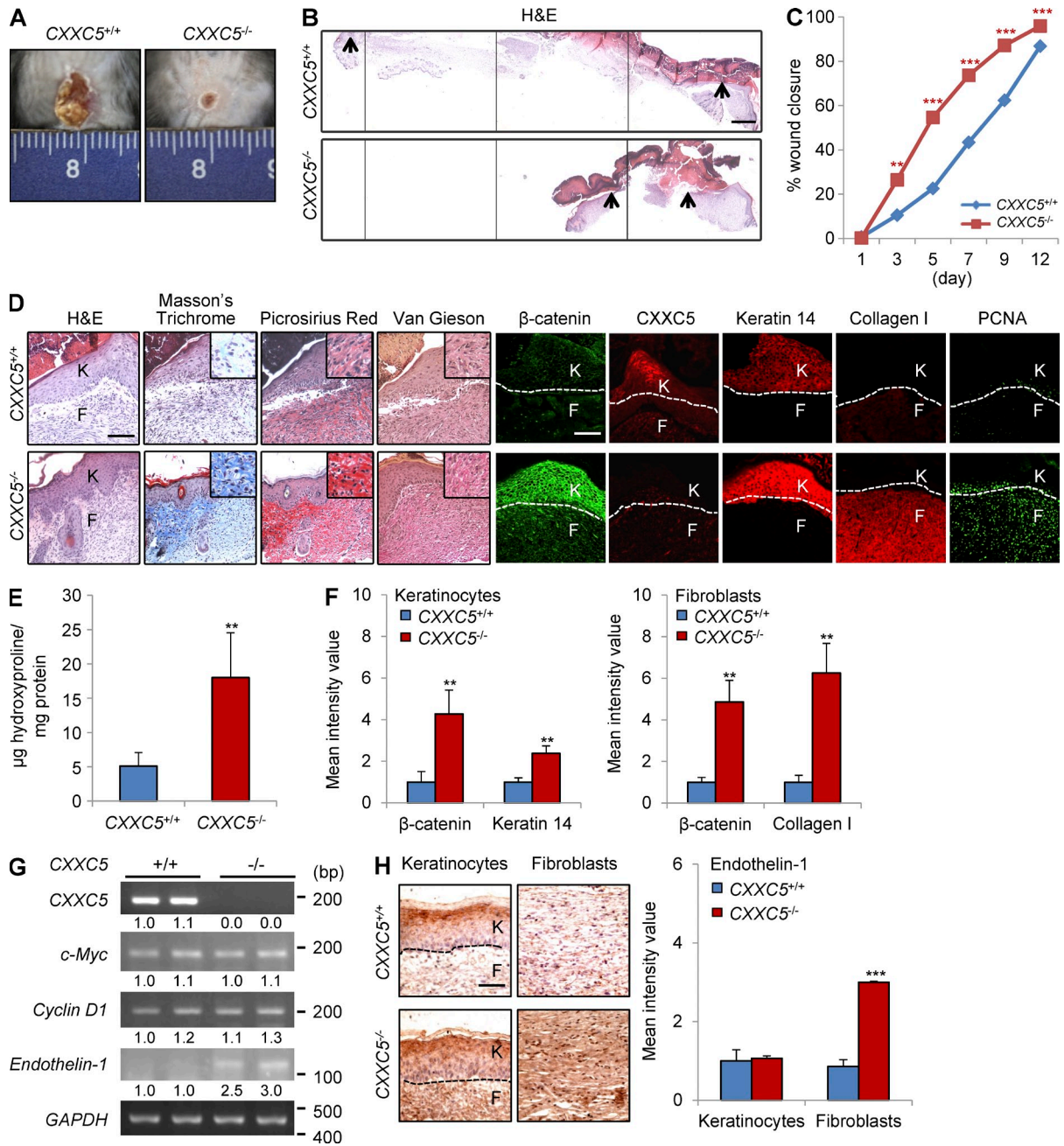
Figure 4. Loss of CXXC5 accelerates cutaneous wound healing and enhances collagen production in mice. A full-thickness wound (diameter = 1.5 cm) was made on the backs of 7-wk-old $CXXC5^{+/+}$ and $CXXC5^{-/-}$ mice ($n = 16$ mice/group). (A and B) Representative macroscopic images (A) and H&E staining (B) of wounded skin of $CXXC5^{+/+}$ and $CXXC5^{-/-}$ mice at 12 d after wounding are shown ($n = 3$ independent experiments). Four continuously captured images were connected for analysis of the entire wound of $CXXC5^{+/+}$ and $CXXC5^{-/-}$ mice. Arrowheads indicate the wound margins. (C) Relative healing of wounds of $CXXC5^{+/+}$ and $CXXC5^{-/-}$ mice were measured at 1, 3, 5, 7, 9, and 12 d after wounding and shown as percent wound closure (**, $P < 0.005$; ***, $P < 0.0005$; $n = 16$ mice/group). (D) Representative images of H&E, Masson's trichrome, picrosirius red, and van Gieson staining and IHC showing β-catenin, CXXC5, keratin 14, collagen I, and PCNA of wound sections from $CXXC5^{+/+}$ and $CXXC5^{-/-}$ mice ($n = 5$ mice/group) are presented ($n = 3$ independent experiments). Insets represent the high magnification images of a region of interest. (E) Hydroxyproline levels in the wounds of $CXXC5^{+/+}$ and $CXXC5^{-/-}$ mice were measured at 12 d after wounding (**, $P < 0.005$; $n = 5$ mice/group). (F) Quantitative TissueFAXS analyses of immunohistochemical staining for β-catenin, keratin 14, and collagen I were performed in keratinocytes (left) and fibroblasts (right) of wounds of $CXXC5^{+/+}$ and $CXXC5^{-/-}$ mice (**, $P < 0.005$; $n = 5$ mice/group) at 12 d after wounding ($n = 3$ independent experiments). (G) RT-PCR analysis was performed with wound tissue obtained from $CXXC5^{+/+}$ and $CXXC5^{-/-}$ mice at 12 d after wounding to detect mRNA levels of CXXC5, endothelin-1, c-Myc, cyclin D1, and GAPDH ($n = 2$ mice/group). Relative densitometry values are shown underneath blot as ratios relative to the levels of GAPDH. (H) IHC staining for endothelin-1 in keratinocytes (left) and fibroblasts (right) of wounds of $CXXC5^{+/+}$ and $CXXC5^{-/-}$ mice ($n = 3$ mice/group; left) and quantitative TissueFAXS analyses of IHC staining for endothelin-1 (right) were performed (***, $P < 0.0005$; $n = 3$ independent experiments). (D and H) Dashed lines demarcate the epidermal–dermal boundary. F, fibroblasts; K, keratinocytes. Bars: (B) 500 μm; (D) 100 μm; (H) 50 μm. Means ± SD.
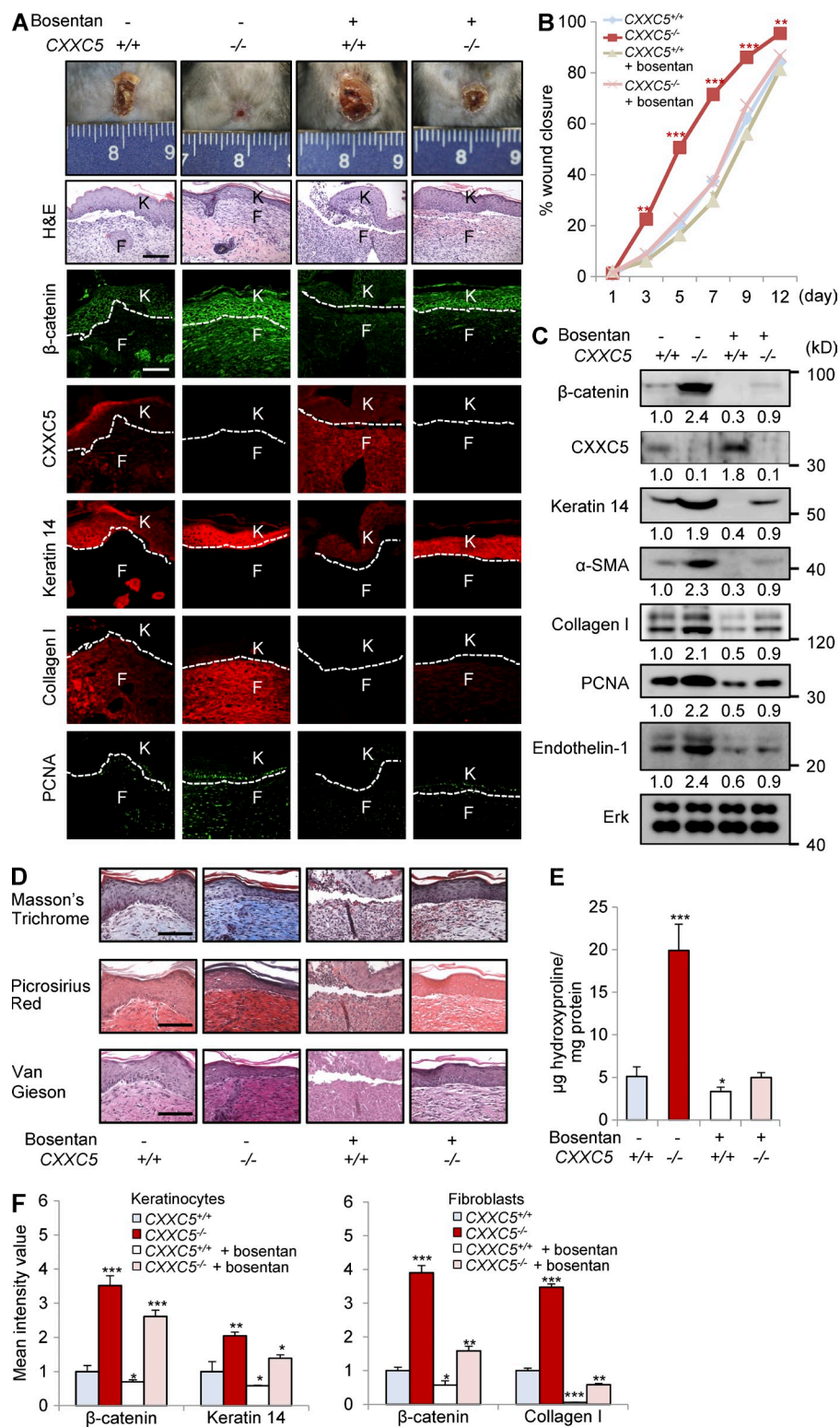
Figure 5. Bosentan alleviates the accelerated wound–healing phenotype of CXXC5−/− mice. After generation of full-thickness wounds (diameter = 1.5 cm) on the backs of CXXC5+/+ and CXXC5−/− mice, the mice were orally administered 100 mg/kg/d bosentan monohydrate daily for 11 d (n = 10 mice/group). (A) Representative images of macroscopic wounds, H&E staining, and IHC staining for β-catenin, CXXC5, keratin 14, collagen I, and PCNA in the wounds of CXXC5+/+ and CXXC5−/− mice treated or untreated with bosentan at 12 d after wounding (n = 4 mice/group) are shown (n = 3 independent experiments). Dashed lines indicate the epidermal–dermal boundary. F, fibroblasts; K, keratinocytes. (B) Relative wound closure rates after bosentan treatment in CXXC5+/+ and CXXC5−/− mice are shown. Wound sizes were measured at 1, 3, 5, 7, 9, and 12 d after wounding (*, P < 0.05; **, P < 0.005; ***, P < 0.0005; n = 10 mice/group). (C) Western blot analyses of wound tissue lysates from CXXC5+/+ and CXXC5−/− mice treated with or without bosentan 12 d after wounding (n = 2 mice/group) were performed to detect β-catenin, CXXC5, keratin 14, α-SMA, collagen I, PCNA, endothelin-1, and Erk (n = 2 independent experiments). Relative densitometric ratios of each protein to Erk protein are shown. (D) Representative images of Masson's trichrome, picrosirius red, or van Gieson staining of wound tissues obtained from CXXC5+/+ and CXXC5−/− mice treated with or without bosentan 12 d after wounding (n = 4 mice/group) are shown (n = 3 independent experiments). (A and D) Bars, 100 µm. (E) Hydroxyproline levels in wounds of CXXC5+/+ and CXXC5−/− mice treated with or without bosentan 12 d after wounding are shown (*, P < 0.05; ***, P < 0.0005; n = 4 mice/group). (F) Quantitative Tissue-FAXS analyses of IHC staining shown in A were performed in keratinocytes (left) and fibroblasts (right; *, P < 0.05; **, P < 0.005; ***, P < 0.0005; n = 3 independent experiments). Means ± SD.

did not affect c-Myc and cyclin D1 (Fig. 7 B). ICC analyses also showed that PTD-DBM increased the nuclear translocation of β-catenin and induced collagen I production (Fig. 7 C). Transfection with β-catenin siRNA caused a reduction in the levels of β-catenin and endothelin-1 in human dermal fibroblasts

(Fig. 7 D). Knockdown of β-catenin abolished the PTD-DBM–induced increases in α-SMA and collagen I (Fig. 7 D). Bosentan also blocked the increases of α-SMA and collagen I induced by PTD-DBM (Fig. 7 E). PTD-DBM induced the Wnt reporter activity, Col1a2 promoter activity, and collagen
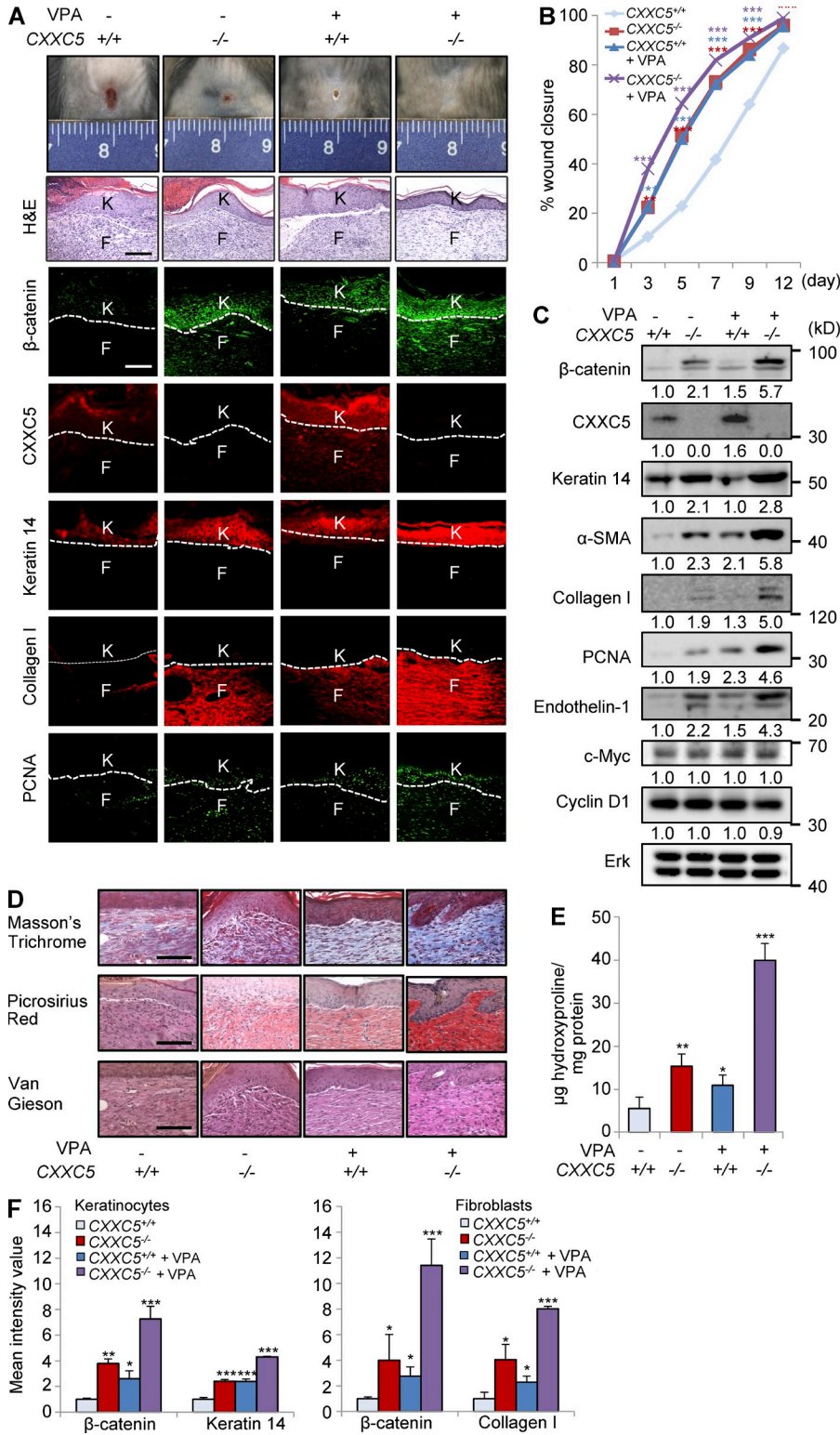
Figure 6. **VPA treatment further accelerates cutaneous wound healing in CXXC5−/− mice.** After generation of full-thickness wounds (diameter = 1.5 cm) on the backs of CXXC5+/+ and CXXC5−/− mice, 500 mM VPA was applied topically to the wounds daily (n = 10 mice/group). (A) Representative images of macroscopic wounds, H&E, and IHC staining showing expression of β-catenin, CXXC5, keratin 14, collagen I, and PCNA in the wounds of CXXC5+/+ and CXXC5−/− mice treated with or without VPA treatment 12 d after wounding (n = 4 mice/group) are shown (n = 3 independent experiments). Dashed lines indicate the epidermal–dermal boundary. F, fibroblasts; K, keratinocytes. (B) Relative wound closure rates describe the effects of VPA on wound healing in CXXC5+/+ and CXXC5−/− mice. Wound sizes were measured at 1, 3, 5, 7, 9, and 12 d after wounding (**, P < 0.005; ***, P < 0.0005; n = 10 mice/group). (C) Western blot analyses of β-catenin, CXXC5, keratin 14, α-SMA, collagen I, PCNA, endothelin-1, c-Myc, cyclin D1, and Erk were performed in wounds of CXXC5+/+ and CXXC5−/− mice treated with or without VPA (n = 2 mice/group) 12 d after wounding (n = 2 independent experiments). Relative densitometry values are shown below blots. (D) Representative images of Masson's trichrome, picrosirius red, or van Gieson staining of wounds of CXXC5+/+ and CXXC5−/− mice treated with or without VPA 12 d after wounding (n = 4 mice/group) are shown (n = 3 independent experiments). (A and D) Bars, 100 μm. (E) Hydroxyproline levels in wounds of CXXC5+/+ and CXXC5−/− mice treated with or without VPA 12 d after wounding are shown (*, P < 0.05; **, P < 0.005; ***, P < 0.0005; n = 4 mice/group). (F) Quantitative TissueFAXS analyses of IHC staining shown in A were performed in keratinocytes (left) and fibroblasts (right; *, P < 0.05; **, P < 0.005; ***, P < 0.0005; n = 3 independent experiments). Means ± SD.

concentration in the supernatants in a dose-dependent manner (Fig. 7 F). The stimulatory effects of PTD-DBM were comparable with those of Wnt3a or TGF-β, which are key mediators of dermal fibrosis (Fig. 7 F; Sato, 2006; Carthy et al.,

2011). PTD-DBM also enhanced the ability of fibroblasts to contract collagen gels (Fig. 7 G). We next investigated the effect of PTD-DBM on fibroblast migration after scratching of cell monolayers. 24 h after PTD-DBM treatment, the numbers
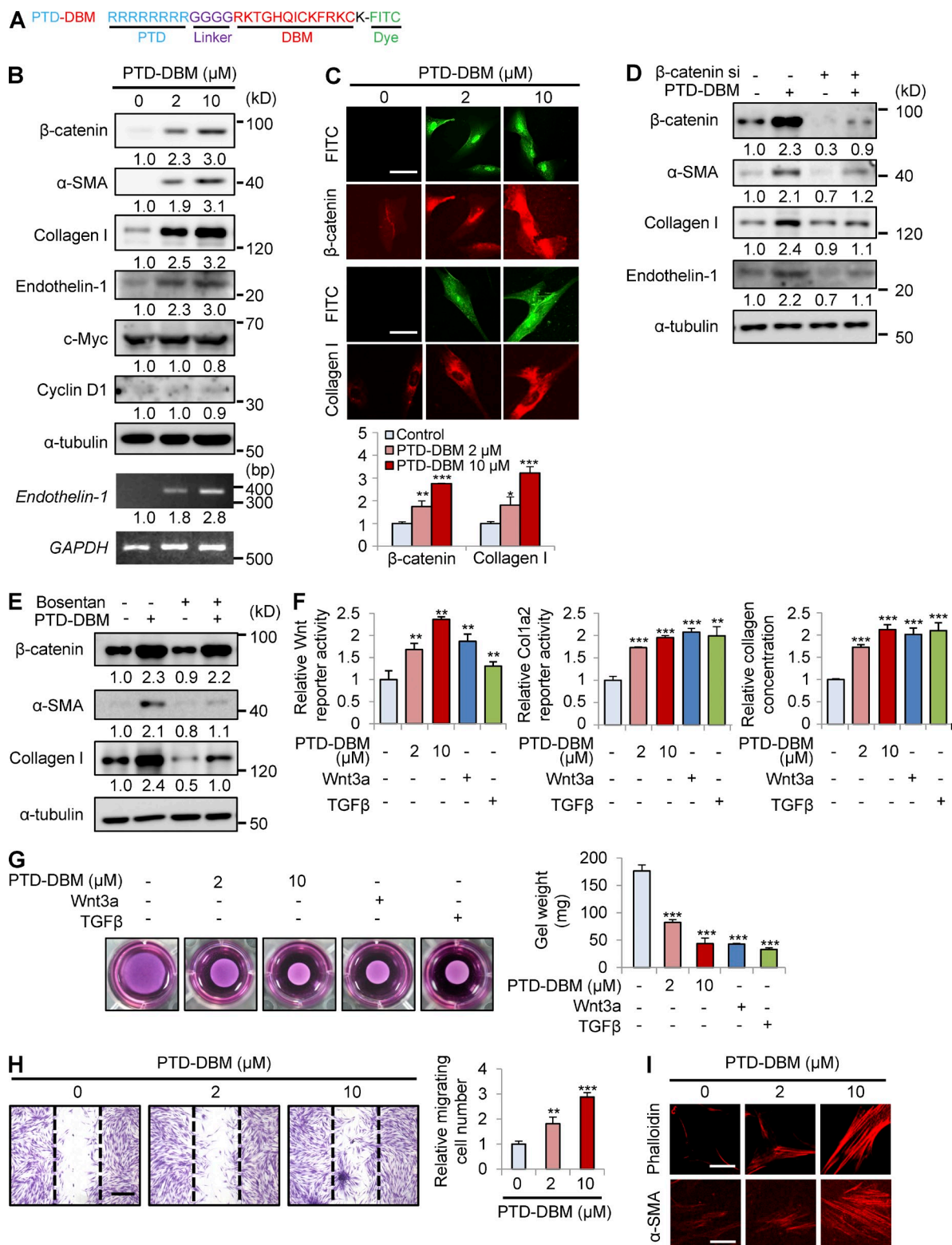
Figure 7. PTD–DBM induces collagen production in human dermal fibroblasts. (A) PTD-DBM is a synthetic peptide that includes a PTD for enhanced protein delivery, a linker for flexibility, DBM, and lysine conjugated with FITC for visualization. (B) Human dermal fibroblasts (n = 2–3 cells), which were treated with 2 or 10 µM PTD-DBM for 2 d, were analyzed using Western blotting to detect β-catenin, α-SMA, collagen I, endothelin-1, c-Myc, cyclin D1, and α-tubulin. *Endothelin-1* and *GAPDH* expression were measured by RT-PCR analysis (n = 2 independent experiments). Relative densitometry values are shown below the blots as ratios relative to the levels of loading control (α-tubulin or *GAPDH*). (C) Human dermal fibroblasts, treated with 2 or 10 µM PTD-DBM

of cells that migrated in the scratched area were significantly increased (Fig. 7 H). In addition, fibroblasts treated with PTD-DBM showed increased stress fibers and a thicker cortical network compared with control fibroblasts as determined by ICC analyses with anti-phalloidin or anti–α-SMA antibody (Fig. 7 I).

Combination treatment with PTD–DBM and Wnt3a synergistically induces expression of β–catenin, α–SMA, and collagen I

The role of CXXC5 as a negative feedback regulator of the Wnt/β-catenin pathway was confirmed by the synergistic increase in β-catenin levels after co-treatment with PTD-DBM and either Wnt3a or VPA (Fig. 8, A and B). Wnt3a or PTD-DBM treatment alone induced α-SMA and collagen I, but combination treatment induced the greatest fibrotic effect in human dermal fibroblasts (Fig. 8 A). Although VPA marginally increased the levels of α-SMA and collagen I, co-treatment with PTD-DBM and VPA also synergistically increased the expression of these markers (Fig. 8 B). We also observed synergistic increases of β-catenin in the nucleus and cytosol via ICC analysis after co-treatment with PTD-DBM and Wnt3a (Fig. 8 C). Moreover, PTD-DBM significantly disrupted the Wnt3a-induced interaction between CXXC5 and Dvl-1 (Fig. 8 D). The synergistic increases in Wnt reporter activity, *Col1a2* reporter activity, and collagen concentration were also observed in fibroblasts treated with both PTD-DBM and Wnt3a (Fig. 8 E). Furthermore, co-treatment with PTD-DBM and Wnt3a significantly induced contraction of collagen gels (Fig. 8 F). Cell migration and stress fiber formation were also synergistically induced by treatment with a combination of PTD-DBM and Wnt3a (Fig. 8, G and H). Co-treatment with PTD-DBM and Wnt3a also significantly increased β-catenin in HaCaT keratinocytes (Fig. 8 I).

Co-treatment with PTD–DBM and VPA accelerates cutaneous wound healing and synergistically induces β–catenin, keratin 14, and collagen I expression in mice

To investigate the effect of co-treatment with PTD-DBM and VPA on cutaneous wound healing in vivo, we created cutaneous wounds (diameter = 1.5 cm) on the dorsal skin of

C3H mice and applied PTD-DBM and/or VPA topically to the wounds on a daily basis. As a positive control, one group of mice was treated with epidermal growth factor (EGF), a currently prescribed wound-healing agent (Kim et al., 2010b, 2014b). When the wounds were treated with PTD-DBM, we observed a strong increase in β-catenin expression (Fig. 9 A). Treatment with PTD-DBM or VPA accelerated cutaneous wound healing as efficiently as EGF (Fig. 9, B–D); however, combination treatment with PTD-DBM and VPA accelerated cutaneous wound healing much more efficiently than treatment with EGF alone (Fig. 9, B–D). The wounds were completely reepithelialized by combination treatment with PTD-DBM and VPA (Fig. 9, B and C) with reduction in inflammatory cells (Fig. 9 C). Notably, the combination treatment group exhibited 42.8% reepithelialization, whereas the control group only exhibited 4.9% reepithelialization 3 d after wounding (Fig. 9 D). Treatment with a combination of PTD-DBM and VPA induced expression of β-catenin, keratin 14, collagen I, endothelin-1, and PCNA much more effectively than treatment with EGF only (Fig. 9, C and E). The levels of phosphorylated ERK induced by the different treatment agents also correlated with the levels of β-catenin and wound-healing markers (Fig. 9, C and E). The combination treatment groups showed higher levels of collagen than other groups, including the EGF treatment group, as determined by collagen staining and hydroxyproline assay (Fig. 9, F and G). Quantitative TissueFAXS analyses also showed that β-catenin and the wound-healing markers were significantly induced in keratinocytes and fibroblasts by treatment with both PTD-DBM and VPA (Fig. 9 H). The more efficient improvement of cutaneous wound healing after combination treatment with PTD-DBM and VPA compared with after EGF treatment was convincingly shown by time course analyses during the wound-healing process (Fig. 10, A and B). However, the levels of c-Myc and cyclin D1 were not obviously changed in all treatment groups (Figs. 9 E and 10 C). Finally, we treated PTD-DBM on the wounds of *Axin2^{LacZ/+}* mice (Gay et al., 2013; Whyte et al., 2013) to monitor the effect of PTD-DBM on Wnt activation in vivo. Axin2-LacZ expression was significantly increased in dermal fibroblasts of wounds treated with PTD-DBM (Fig. 10 D).

for 2 d, were subjected to ICC analyses to detect β-catenin or collagen I. Representative ICC images are shown (top), and mean intensity values are presented (bottom; *, P < 0.05; **, P < 0.005; ***, P < 0.0005; n = 3 independent experiments). (D) Human dermal fibroblasts were treated with PTD-DBM for 2 d after treatment with β-catenin siRNA (β-catenin si). Western blot analyses of WCLs were performed with antibodies against β-catenin, α-SMA, collagen I, endothelin-1, or α-tubulin (n = 2 independent experiments). (E) Human dermal fibroblasts, treated with 2 µM PTD-DBM and/or 10 µM bosentan for 2 d, were analyzed by Western blotting to detect β-catenin, α-SMA, collagen I, and α-tubulin (n = 2 independent experiments). (D and E) Relative densitometry values are shown below the blots. (F) Wnt reporter activity (left), *Col1a2* reporter activity (middle), and the concentration (right) of collagen in the supernatants of human dermal fibroblasts were measured after treatment with 2 or 10 µM PTD-DBM, 50 ng/ml Wnt3a, or 10 ng/ml TGF-β (**, P < 0.005; ***, P < 0.0005; n = 3 independent experiments). (G) A collagen gel contraction assay after treatment with 2 or 10 µM PTD-DBM, 50 ng/ml Wnt3a, or 10 ng/ml TGF-β was performed and representative images are shown (left). Gel weight quantitation is shown (right; ***, P < 0.0005; n = 3 independent experiments). (H) An in vitro wound healing assay was performed after treatment with or without 2 or 10 µM PTD-DBM. Representative images (left) and migrating cell numbers (right) are shown (**, P < 0.005; ***, P < 0.0005; n = 3 independent experiments). The widths of the wounds scratched at the start of the assay are indicated with dashed lines. (I) ICC staining for phalloidin (left) and α-SMA (right) was performed in human dermal fibroblasts treated with or without 2 or 10 µM PTD-DBM. Representative ICC images are shown (n = 3 independent experiments). Bars: (C and I) 50 µm; (H) 500 µm. Means ± SD.
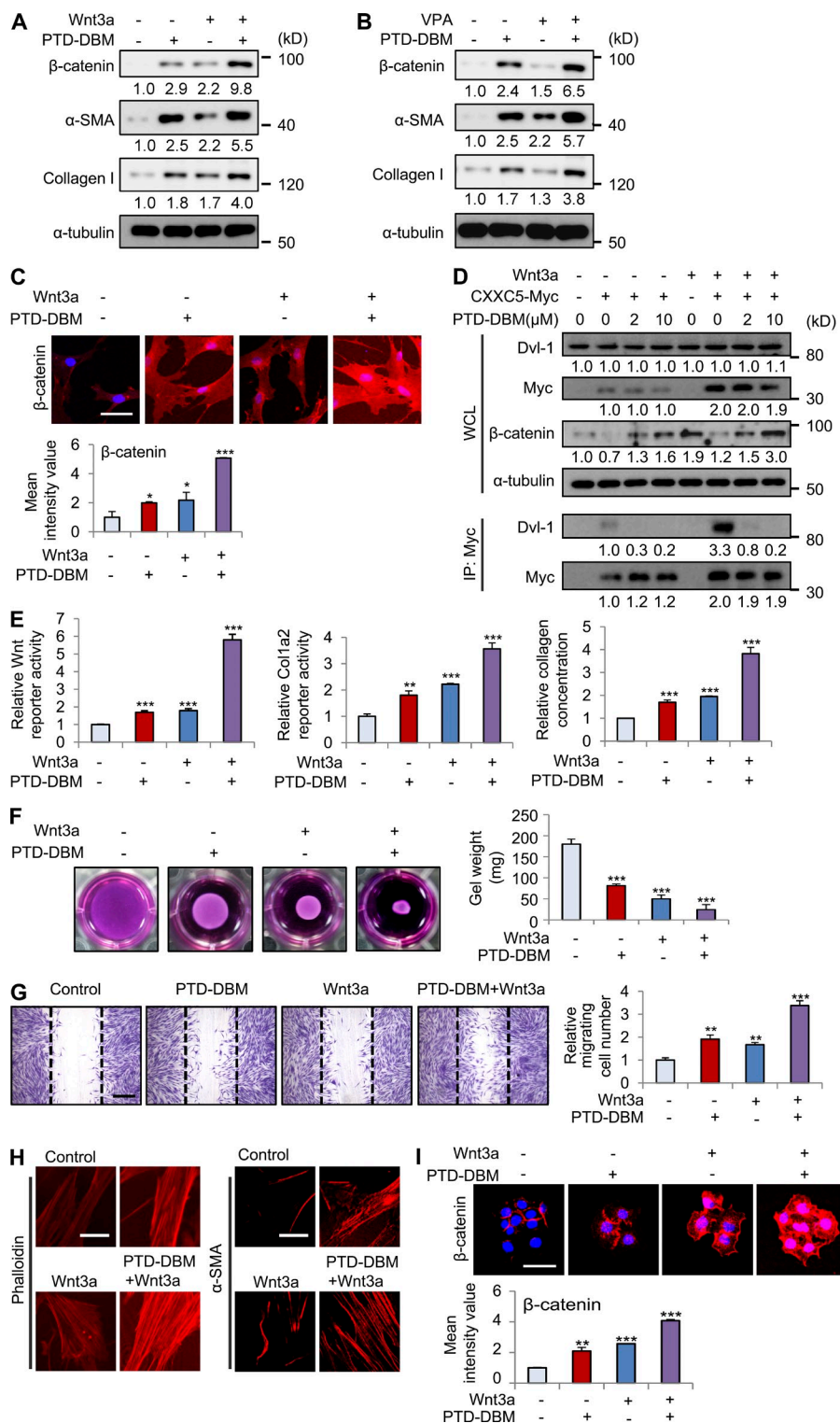
Figure 8.   Combination treatment with PTD–DBM and Wnt3a synergistically induces collagen production in human dermal fibroblasts. (A) Human dermal fibroblasts ($n = 2$–3 cells) were treated with 2 µM PTD-DBM and/or 50 ng/ml Wnt3a for 2 d. (B) Human dermal fibroblasts were treated with 2 µM PTD-DBM and/or 1 mM VPA for 2 d. (A and B) WCLs were subjected to Western blotting to detect β-catenin, α-SMA, collagen I, and α-tubulin ($n = 2$ independent experiments). Relative densitometric ratios of each protein to α-tubulin are shown. (C) Representative images of ICC staining of β-catenin (top) in human dermal fibroblasts, which were treated with 2 µM PTD-DBM and/or 50 ng/ml Wnt3a, and mean intensity value (bottom) are shown (*, $P < 0.005$; ***, $P < 0.0005$; $n = 3$ independent experiments). (D) Human dermal fibroblasts were treated with 2 µM PTD-DBM and/or 50 ng/ml Wnt3a after transfection with pcDNA3.1 or pcDNA3.1-CXXC5-Myc. The cell lysates were used for immunoprecipitation with anti-Myc antibody ($n = 2$ independent experiments). Relative densitometry values are shown below the blots. (E) Wnt reporter assay, *Col1a2* reporter assay, and Sircol collagen assay in human dermal fibroblasts treated with PTD-DBM and/or Wnt3a were measured (**, $P < 0.005$; ***, $P < 0.0005$; $n = 3$ independent experiments). (F) A collagen gel contraction assay in human dermal fibroblasts treated with PTD-DBM and/or Wnt3a was performed, and representative images are shown (left). Gel weight quantitation is also shown (right; ***, $P < 0.0005$; $n = 3$ independent experiments). (G) An in vitro wound healing assay in human dermal fibroblasts treated with PTD-DBM and/or Wnt3a was performed. Representative images (left) and migrating cell numbers (right) are shown (**, $P < 0.005$; ***, $P < 0.0005$; $n = 3$ independent experiments). The widths of the initially scratched wounds are indicated with dashed lines. (H) ICC staining of human dermal fibroblasts treated with PTD-DBM and/or Wnt3a was performed to detect phalloidin (left) and α-SMA (right; $n = 3$ independent experiments). (I) Representative images of ICC staining of β-catenin (top) are shown in HaCaT keratinocytes, which were treated with 2 µM PTD-DBM and/or 50 ng/ml Wnt3a. Mean intensity values are shown below (**, $P < 0.005$; ***, $P < 0.0005$; $n = 3$ independent experiments). Bars: (C, H, and I) 50 µm; (G) 500 µm. Means ± SD.

DISCUSSION

TGF-β has been implicated as a major signaling molecule involved in both cutaneous wound healing and dermal fibrosis (Diegelmann and Evans, 2004). Recent studies have shown that the interaction between the Wnt/β-catenin pathway and TGF-β is important for cutaneous wound healing and fibrosis (Carthy et al., 2011; Akhmetshina et al., 2012). Wnt3a induces myofibroblast differentiation by up-regulating
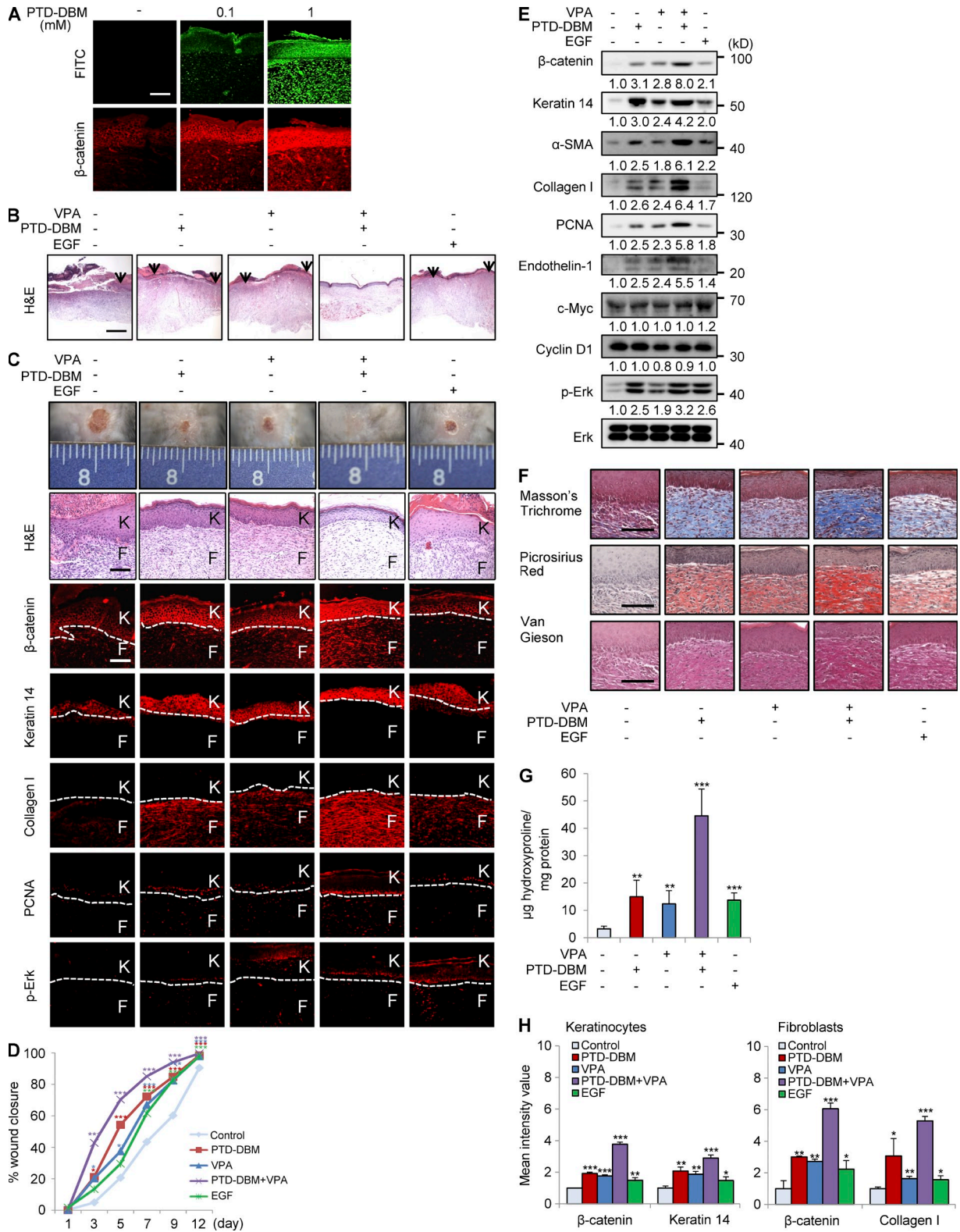
Figure 9. Co–treatment with PTD–DBM and VPA accelerates cutaneous wound healing and synergistically induces collagen production in mice. The wounded skin of 7-wk-old male C3H mice was treated daily with 100 µM PTD-DBM and/or 500 mM VPA or with 100 µM EGF for 11 d ($n = 16$ mice/group). (A) IHC staining of wounds treated with PTD-DBM was performed to detect β-catenin. Representative images are shown ($n = 3$ independent experiments). (B) Representative H&E-stained images of wounds at 12 d after wounding with the different treatments are shown ($n = 3$ independent experiments). The arrowheads represent the edges of the wounds. (C) Representative images of macroscopic wounds and H&E and IHC staining ($n = 5$

the TGF-β pathway through Smad 2 in a β-catenin–dependent manner (Carthy et al., 2011). TGF-β also stimulates the Wnt/β-catenin pathway by inhibiting GSK3β or decreasing Dickkopf-1 (Dkk-1) expression (Cheon et al., 2004; Amini Nik et al., 2007; Akhmetshina et al., 2012). The cross-talk between the Wnt/β-catenin and TGF-β pathways indicates that control of the Wnt/β-catenin pathway may be an effective approach for targeting the TGF-β pathway in cutaneous wound healing and dermal fibrosis.

Several negative regulators of the Wnt/β-catenin pathway inhibit cutaneous wound healing and dermal fibrosis. For example, Dkk-1, a Wnt/β-catenin pathway antagonist (Niida et al., 2004), decreases the proliferation of dermal fibroblasts and suppresses the phenotypes of pachydermoperiostosis (Kabashima et al., 2010). Overexpression of Dkk-1 also prevents fibrosis in vitro and in vivo (Akhmetshina et al., 2012). As a second example, blocking of secreted frizzled–related protein 1 (SFRP1), a negative regulator of the Wnt/β-catenin pathway (Gaur et al., 2006), with anti-SFRP1 antibody promotes wound healing in vivo (Li and Amar, 2006). Furthermore, SFRP1 inhibits β-catenin expression, cellular growth, and ECM production in keloid fibroblasts (Chua et al., 2011). Inhibition of GSK3β, a negative Wnt regulator (Eisenmann, 2005), enhances wound healing and collagen deposition (Bergmann et al., 2011).

We demonstrated that CXXC5 functions as a negative feedback regulator of the Wnt/β-catenin pathway and collagen production in the wound-healing process. The enhancement of wound healing in *CXXC5*$^{-/-}$ mice and identification of the role of CXXC5 as a negative regulator of the Wnt/β-catenin pathway indicate that blockade of the CXXC5-Dvl interaction may be a potential strategy for the development of novel drugs for the treatment of acute wounds. We confirmed that the CXXC5-Dvl interaction is a plausible target for development of wound healing agents by demonstrating beneficial effects of PTD-DBM, a competitor peptide which interrupts this CXXC5-Dvl interaction, on cutaneous wound healing and collagen deposition. Importantly, we observed further improvement in the wound-healing effect after simultaneous blocking of the negative feedback loop with PTD-DBM and activation of the Wnt/β-catenin pathway with Wnt3a or VPA.

In addition, the wounds of *Axin2*$^{LacZ/+}$ mice treated with PTD-DBM showed a significant increment of Wnt activity in the dermal fibroblasts during cutaneous wound healing. Although there are slight variations of activity levels with the wounds in other references (Gay et al., 2013; Whyte et al., 2013), these results are still correlated. Endothelin-1, a target of Wnt/β-catenin pathway, was also specifically increased in the fibroblasts of *CXXC5*$^{-/-}$ mouse wounds. Collectively, Wnt/β-catenin signaling is important in the promotion of cutaneous wound healing by CXXC5 manipulation in the dermal fibroblasts of wounds.

Large wounds show somehow a nonuniform rate of contraction, as shown in the representative macroscopic images of mouse wounds in our manuscript. Despite the nonuniform rate of contraction in large wounds, research on clinical treatment of the large wounds, including surgical wounds, is valuable. To overcome this problem, we performed quantitative analysis and diverse methodologies for the evaluation of healing, including quantitation of collagen. Combination treatment with PTD-DBM and VPA significantly induced reepithelialization and enhanced collagen deposition in the large wounds.

A topical treatment is commonly used for treatment of cutaneous wound healing (Kim et al., 2010b; Chen et al., 2012; Tang et al., 2014). For efficient skin penetration, there are many methodologies, including PTD conjugation (Zhang et al., 2014), liposomalization (Whyte et al., 2013), and use of penetration enhancers (Lan et al., 2014). Considering the skin penetration efficiency, we used PTD for efficient delivery and FITC for visualization. Our data demonstrated that PTD-DBM efficiently delivered to cells both in vitro and in vivo.

Previous studies have described an increased risk of basal cell carcinoma in association with both acute and chronic wounds (Özyazgan and Kontaş, 2004; Kasper et al., 2011). Considering this relationship between epidermal wounds and skin cancer risk, we investigated the effect of CXXC5 on cancer risk during wound healing. PTD-DBM did not increase expression levels of two oncogenic markers, c-Myc and cyclin D1 (Liao et al., 2007), in vitro and in vivo. Moreover, expression of endothelin-1 but not of c-Myc or cyclin D1 was significantly increased in *CXXC5*$^{-/-}$ mice. We also found no abnormal skin phenotypes without increased expression of c-Myc or cyclin D1 after PTD-DBM treatment for 6 mo (Fig. 10 E). Finally, activation of the Wnt/β-catenin pathway via disruption of the negative feedback loop rather than by direct activation of signaling may further reduce the chance of aberrant activation of the Wnt/β-catenin pathway related to cancer.

mice group) for β-catenin, keratin 14, collagen I, PCNA, or p-Erk in wounds 12 d after wounding are shown. Dashed lines demarcate the epidermal–dermal boundary ($n = 3$ independent experiments). F, fibroblasts; K, keratinocytes. (D) Relative wound closure rates for wounds from mice treated with PTD-DBM and/or VPA or EGF were quantified as percent wound closure as shown. Wound sizes were measured at 1, 3, 5, 7, 9, and 12 d after wounding (*, $P < 0.05$; **, $P < 0.005$; ***, $P < 0.0005$; $n = 16$ mice/group). (E) Western blot analyses of β-catenin, keratin 14, α-SMA, collagen I, PCNA, endothelin-1, c-Myc, cyclin D1, p-Erk, and Erk in wounds ($n = 2$ mice/group) 12 d after wounding were performed ($n = 2$ independent experiments). Relative densitometric ratios of each protein to Erk protein are shown. (F) Representative images of Masson's trichrome, picrosirius red, and van Gieson staining of wounds ($n = 5$ mice/group) 12 d after wounding are shown ($n = 3$ independent experiments). Bars: (A, C, and F) 100 μm; (B) 500 μm. (G) Hydroxyproline levels were measured in wounds at 12 d after wounding (**, $P < 0.005$; ***, $P < 0.0005$; $n = 5$ mice/group). (H) Quantitative TissueFAXS analyses of immunohistochemical staining shown in C are presented for keratinocytes (left) and fibroblasts (right; *, $P < 0.05$; **, $P < 0.005$; ***, $P < 0.0005$; $n = 3$ independent experiments). Means ± SD.
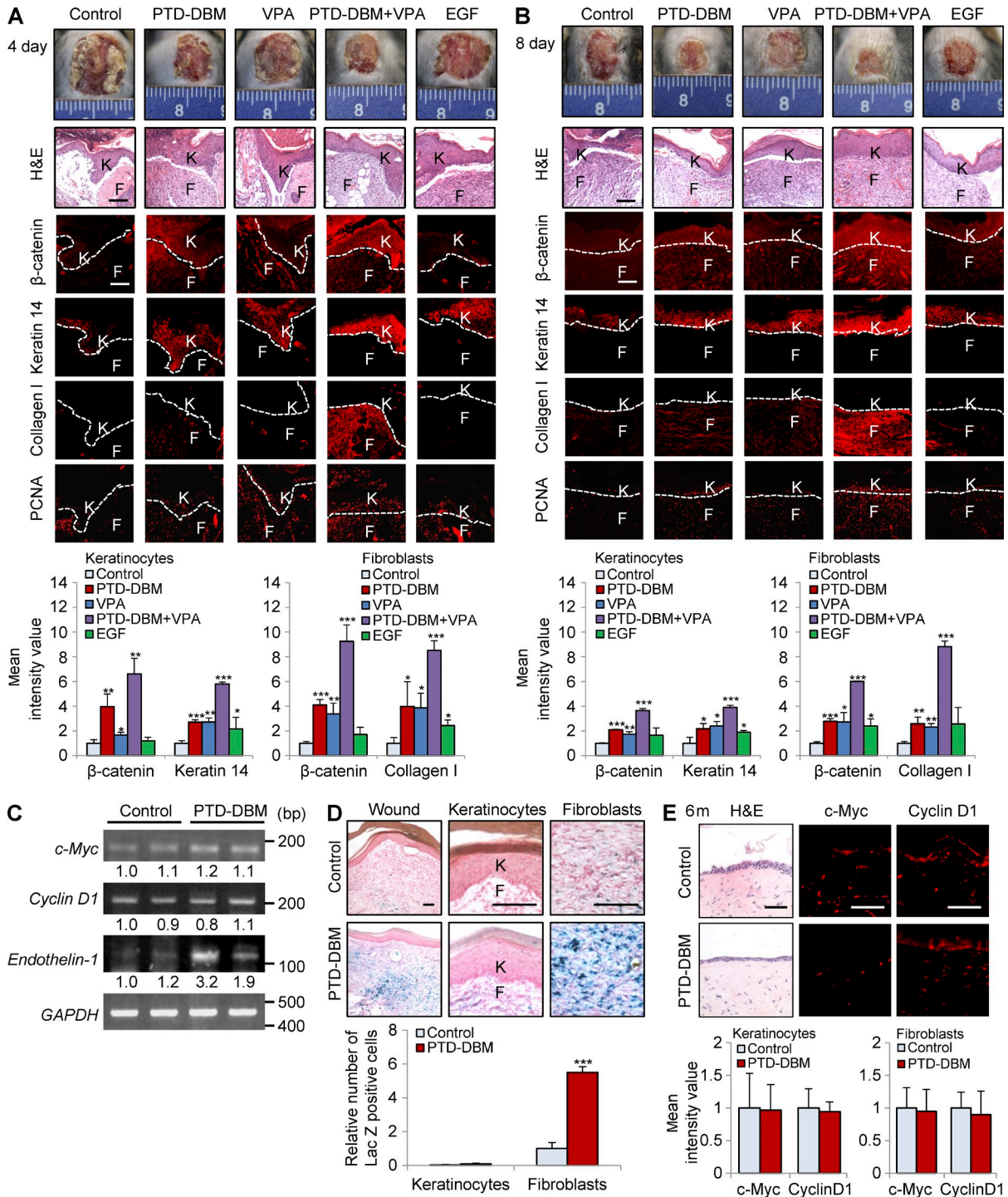
Figure 10.   PTD–DBM induces β–catenin, wound–healing markers, and endothelin–1 during cutaneous wound healing. (A and B, top) Representative images of macroscopic wounds, H&E staining and IHC staining for β-catenin, keratin 14, collagen I, or PCNA in wounds (n = 3 mice group) 4 (A) and 8 d (B) after wounding are shown. Dashed lines demarcate the epidermal–dermal boundary. F, fibroblasts; K, keratinocytes. (bottom) Mean intensity values are presented for keratinocytes (left) and fibroblasts (right; *, P < 0.05; **, P < 0.005; ***, P < 0.0005; n = 3 independent experiments). (C) RT-PCR analysis was performed 12 d after wounding on wounds treated with or without 100 µM PTD-DBM to detect the mRNA levels of *CXXC5*, *endothelin-1*, *c-Myc*, *cyclin D1*, and *GAPDH* (n = 2 mice/group). Relative densitometry values are shown underneath the blots. (D, top) Representative images of X-gal staining of wounded tissue from *Axin2^LacZ/+* mice (n = 3 mice/group) treated with 100 µM PTD-DBM for 11 d and magnified images in epidermal keratinocytes and dermal fibroblasts are shown. (bottom) Relative number of lacZ-positive cells is presented in keratinocytes and fibroblasts (***, P < 0.0005; n = 3 independent experiments). (E) Representative images of H&E staining and IHC staining for c-Myc or cyclin D1 in wounds (n = 3 mice/group) at 6 mo after wounding (top) and mean intensity values are presented for keratinocytes (left) and fibroblasts (right; bottom) are shown (n = 3 independent experiments). Bars: (A, B, and D) 100 µm; (E) 50 µm. Means ± SD.

In conclusion, CXXC5 is a negative regulator of cutaneous wound healing and collagen production and functions via inhibition of the Wnt/β-catenin pathway. The PTD-DBM peptide blocks the CXXC5-Dvl interaction, and combination treatment with this peptide and a Wnt/β-catenin signaling activator may represent a potential therapeutic strategy to enhance cutaneous wound healing without side effects and with minimal cost.

MATERIALS AND METHODS

Human skin specimens. To monitor the expression patterns of β-catenin and CXXC5 during the wound-healing process, 4-mm biopsy specimens from acute wounds were derived from wound margins of five patients at 0, 7, 28, and 84 d after primary excision of cutaneous melanoma. The specimens at 0 d are intact and normal skins. The tissue specimens were fixed overnight in 10% (vol/vol) formalin in PBS for immunohistochemical analyses. Experiments using patient samples were approved by the Institutional Review Board of the Clinical Research Institute of Severance Hospital (approval no. 4-2011-0690) and were conducted according to the Declaration of Helsinki Principles.

In vivo wound healing assay. 7-wk-old male C3H mice (Orient Bio Co.) were used to confirm the synergistic effect of PTD-DBM and VPA on cutaneous wound healing. Mice were anesthetized, and their backs were shaved and cleaned with ethanol. Full-thickness incision wounds (diameter = 1.5 cm) were generated and treated daily with 100 µM PTD-DBM alone, 500 mM VPA alone (Acros), PTD-DBM and VPA in combination, or 100 µM EGF alone (PeproTech; n = 16 per group). As a control, one group of mice was treated with vehicle (PBS) only.

For generation of $CXXC5^{-/-}$ mice (Kim et al., 2014a), $CXXC5$-targeted CJ7 mouse embryonic stem cell clones were injected into C57BL/6 mouse blastocysts. Chimeric offspring were bred to C57BL/6 mice to obtain heterozygotes for the $CXXC5$ mutation. To obtain littermate wild-type and $CXXC5^{-/-}$ mice, $CXXC5$ heterozygous mice were intercrossed for four generations. Experiments were performed on littermate $CXXC5^{+/+}$ and $CXXC5^{-/-}$ mice in an identical way to normal mice. To investigate whether the accelerated wound-healing phenotype was dependent on endothelin-1, mice were orally administered 100 mg/kg/d bosentan monohydrate or gum Arabic (vehicle; Sigma-Aldrich) for 11 d after wounding.

$Axin2^{LacZ/+}$ mice were purchased from the Jackson Laboratory, and full-thickness incision wounds (diameter = 1.5 cm) were generated and were treated daily with PTD-DBM or vehicle for 11 d (n = 3 per group). All animal protocols were approved by the Institutional Review Board of Severance Hospital, Yonsei University College of Medicine (09-013).

Cell culture, transfection, and in vitro wound healing assay. Human dermal fibroblasts (n = 3) and HaCaT keratinocytes (n = 1) were maintained in DMEM (Gibco) containing 10% (vol/vol) heat-inactivated FBS (Gibco), 100 mg/ml penicillin (Gibco), and 100 mg/ml streptomycin (Gibco) and incubated in 5% (vol/vol) CO_2 at 37°C. For transient transfection, the cells were grown for 1 d, transfected with the required plasmids or siRNAs using the Altogen fibroblast transfection reagent according to the manufacturer's instructions (Altogen Biosystems), and then further cultured for 2 d before harvesting. Human-specific $CXXC5$ siRNAs (5′-CUCAGUGGCAGAUGACACAUU-3′ and 5′-GCACCCGUCUUUA-GAACCAUU-3′) were synthesized (Bioneer) for knockdown of CXXC5. For the in vitro wound healing assay, human dermal fibroblasts or HaCaT keratinocytes were seeded in 12-well plates in DMEM supplemented with 10% FBS and allowed to adhere overnight. The monolayers were then carefully scratched with sterile pipette tips and incubated with medium containing 5% FBS with or without PTD-DBM (2 or 10 µM). After 24 h, the cells were washed once with cold PBS, fixed in 4% paraformaldehyde (PFA) for 15 min at room temperature, and stained with 2% (wt/vol) crystal violet.

Collagen gel contraction assay. 12-well plates were incubated with 1% BSA for 1 h at 37°C. Before the collagen gel contraction assay, human dermal fibroblasts were treated with PTD-DBM or Wnt3a or transfected with pcDNA3.0-CXXC5-Flag. The cells were trypsinized, counted, and resuspended in DMEM at a cell density of 10^5 cells/ml. Thereafter, equal volumes of cells and 0.5 mg/ml type I collagen solution (BD) were mixed together, and then each cell-collagen mixture was added to BSA-coated plates. Collagen was allowed to polymerize for 1 h at 37°C. Fresh DMEM was then added to the solidified collagen gels. Collagen gel contraction was monitored as a loss in gel weight.

Wnt reporter assay. Human dermal fibroblasts were plated in 24-well plates at a density of 5×10^4 cells/well. The cells were transfected with 0.4 µg of the reporter construct TOPFlash or FOPFlash. Luciferase activities were measured using a FLUOstar OPTIMA luminometer. Wnt reporter activities are presented as TOPFlash/FOPFlash.

Col1a2 promoter reporter assay. A luciferase reporter construct under control of the −353-bp to 58-bp $Col1a2$ promoter was obtained from J.H.W. Distler (University of Erlangen-Nuremberg, Erlangen and Nuremberg, Germany; Akhmetshina et al., 2012). Human dermal fibroblasts were plated in 24-well plates at a density of 5×10^4 cells/well. The cells were transfected with 0.4 µg of a Col1a2-luciferase construct using the Altogen fibroblast transfection reagent and then further cultured for 24 h before harvesting. A β-galactosidase reporter vector was used as a control. Luciferase and β-galactosidase activities were measured using a FLUOstar OPTIMA luminometer (BMG LABTECH GMBH).

Sircol collagen assay. The total soluble collagen concentration in the cell supernatants was quantified using the Sircol collagen assay kit (Biocolor Ltd.). The collected supernatants were centrifuged at 200 g for 5 min to remove the ECM, and then 200 µl of the supernatants was mixed with 1 ml Sircol dye for 30 min. The samples were then centrifuged at 9,500 g for 10 min to pack the collagen–dye complex at the bottom of the centrifuge tube. The pellets were dissolved in an alkali reagent to release the collagen–dye complex, and absorbance was then measured at 540 nm using a FLUOstar OPTIMA luminometer.

Hematoxylin and eosin (H&E) staining. Tissues were fixed overnight in 4% (wt/vol) PFA in PBS, embedded in paraffin, and then sliced into 4-µm sections. The sections were deparaffinized in three changes of xylene and rehydrated through a graded ethanol series. The sections were stained with hematoxylin for 5 min and with eosin for 1 min. The H&E-stained slides were photographed using a brightfield optical microscope (ECLIPSE TE2000-U; Nikon).

Immunohistochemistry (IHC). 4-µm paraffin sections were deparaffinized and rehydrated. For antigen retrieval, the slides were autoclaved in 10 mM sodium citrate buffer. Sections were blocked in PBS containing 10% BSA at room temperature for 30 min. The sections were incubated overnight at 4°C with the following dilutions of primary antibodies: anti–β-catenin (1:100; BD), anti-CXXC5 (1:50; Santa Cruz Biotechnology, Inc.), anti–keratin 14 (1:1,000; Covance), anti–collagen I (1:500; Abcam), anti-PCNA (1:500; Santa Cruz Biotechnology, Inc.), anti-vimentin (1:250; Abcam), anti-CD34 (1:500; Abcam), anti-CD68 (1:200; Abcam), and anti–p-Erk (1:50; Cell signaling Technology). The slides were washed with PBS, incubated with Alexa Fluor 488– or Alexa Fluor 555–conjugated IgG secondary antibody (1:400; Molecular Probes) at room temperature for 1 h, and counterstained with DAPI (1:5,000; Boehringer Mannheim). The images were captured using a LSM510 META confocal microscope (Carl Zeiss) after excitation with 405-, 488-, or 543-nm laser lines.

Immunocytochemistry. Human dermal fibroblasts or HaCaT cells were plated in 24–well culture plates. The cells were washed with PBS and fixed in 4% (wt/vol) PFA in PBS for 15 min at room temperature. Then the cells were washed with PBS and permeabilized with 0.1% (vol/vol) Triton X-100 in PBS for 15 min. After washing with PBS, the cells were incubated with 10% BSA in PBS for 30 min and then with antibodies specific for β-catenin (1:100; BD), CXXC5 (1:50; Santa Cruz Biotechnology, Inc.), keratin 14 (1:1,000; Covance), collagen I (1:500; Abcam), phalloidin (1:200; Molecular Probes), or α-SMA (1:200; Abcam) at 4°C overnight. The cells were washed in PBS and incubated with Alexa Fluor 488– or Alexa Fluor 555–conjugated IgG secondary antibody (1:400; Molecular Probes) at room temperature for 1 h. Cell nuclei were counterstained with DAPI for 10 min and the stained samples were examined under a LSM510 META microscope using 405-, 488-, or 543-nm laser excitation lines.

Western blot analysis. Cells and tissues were ground with a mortar and pestle before lysis in RIPA buffer (150 mM NaCl, 10 mM Tris, pH 7.2, 0.1% SDS, 1.0% Triton X-100, 1% sodium deoxycholate, and 5 mM EDTA). Samples were separated on 6–12% SDS polyacrylamide gels and transferred onto PROTRAN nitrocellulose membranes (Schleicher and Schuell Co.). After blocking with PBS containing 5% nonfat dry skim milk and 0.07% (vol/vol) Tween 20, the membranes were incubated with antibody specific for β-catenin (1:1,000; Santa Cruz Biotechnology, Inc.), CXXC5 (1:500; Santa Cruz Biotechnology, Inc.), α-SMA (1:1,000; Abcam), keratin 14 (1:1,000; Covance), collagen I (1:2,000; Abcam), PCNA (1:500; Santa Cruz Biotechnology, Inc.), α-tubulin (1:5,000; Oncogene Research Products), lamin A/C (1:1,000; Cell Signaling Technology), Flag (1:5,000; Sigma-Aldrich), Myc (1:5,000; Cell Signaling Technology), endothelin-1 (1:3,000; Abcam), c-Myc (1:500; Santa Cruz Biotechnology, Inc.), cyclin D1 (1:500; Santa Cruz Biotechnology, Inc.), p-Erk (1:500; Santa Cruz Biotechnology, Inc.), or Erk (1:5,000; Santa Cruz Biotechnology, Inc.) at 4°C overnight. Samples were then incubated with horseradish peroxidase–conjugated anti–rabbit (1:5,000; Bio-Rad Laboratories) or anti–mouse (1:5,000; Cell Signaling Technology) IgG secondary antibody. Protein bands were visualized with enhanced chemiluminescence (GE Healthcare) using a luminescent image analyzer, LAS-3000 (Fujifilm). Western blot bands were analyzed using Multi–Gauge V3.0 software (Fujifilm). Points of interest (POIs) from Western blot bands were marked and quantified using densitometry, and the background signals were subtracted from respective Western blot signals. Relative densitometry values are presented as the intensity ratios of each protein to loading control protein (α-tubulin, lamin A/C, or Erk).

RT-PCR. Total RNA was extracted from cells or ground tissue powder using the TRIzol reagent (Invitrogen). RT was performed using M-MLV reverse transcription (Invitrogen). PCR reactions were performed using Taq DNA polymerase (COSMO Genetech) at 94°C for 5 min followed by 25–40 cycles of 94°C for 30 s, 55–60°C for 30 s, and 72°C for 1 min in a System 2700 thermal cycler (Applied Biosystems). The following primer sets were used: human *CXXC5*, forward 5′-AGCCGAGTGAAGACATTTC-CACCT-3′ and reverse 5′-TAATGAAGAGGCCTGGGTTGATGG-3′; mouse *CXXC5*, forward 5′-CAAGAAGAAGCGGAAACGCTGC-3′ and reverse 5′-TCTCCAGAGCAGCGGAAGGCTT-3′; human *GAPDH*, forward 5′-AAGGTCGGAGTCAACGGATT-3′ and reverse 5′-AGT-GATGGCATGGACTGTGG-3′; mouse *GAPDH*, forward 5′-ACCA-CAGTCCATGCCATCAC-3′ and reverse 5′-TCCACCACCCTG-TTGCTGTA-3′; human *endothelin-1*, forward 5′-TTCCCACAAAGG-CAACAGACCG-3′ and reverse 5′-GACAGGCCCCGAAGTCTGTCA-3′; mouse *endothelin-1*, forward 5′-ACTTCTGCCACCTGGACATC-ATCT-3′ and reverse 5′-TGGTCTGTGGCCTTATTGGGAAGT-3′; mouse *c-Myc*, forward 5′-TGGTGTCTGTGGAGAAGAGGCAAA-3′ and reverse 5′-TTGGCAGCTGGATAGTCCTTCCTT-3′; and mouse *cyclin D1*, forward 5′-TGCTGCAAATGGAACTGCTTCTGG-3′ and reverse 5′-TACCATGGAGGGTGGGTTGGAAAT-3′.

Immunoprecipitation. Cells were lysed in RIPA buffer and centrifuged at 14,000 g for 30 min at 4°C. Cell lysates were then subjected to immunoprecipitation with anti-Myc (1:250; Abcam) or anti–Dvl-1 (1:250; Santa Cruz Biotechnology, Inc.) antibody and Protein A or G beads (GenDEPOT) overnight at 4°C with constant agitation. The immunoprecipitated complexes were washed with RIPA buffer, and the complex samples were boiled and subjected to Western blot analysis.

Collagen staining. 4-μm wound tissue sections were deparaffinized in xylene and rehydrated by successive immersion in descending concentrations of alcohol. To assess the effects of CXXC5 on collagen synthesis and quality of scarring, sections were stained using three common collagen staining methods. For van Gieson staining, slides were stained with Weigert's solution for 10 min and picrofuchsin solution for 2 min. Van Gieson staining results in a deep red color for mature collagen fibers and a pink color for immature collagen fibers along with black nuclei. For Masson's trichrome staining, slides were fixed in Bouin's solution for 1 h. After incubation in Weigert's iron hematoxylin solution for 10 min, the slides were stained with Biebrich Scarlet-Acid Fuchsin and Aniline blue for 5 min. The collagen fibers were stained blue and the nuclei were stained black. For picrosirius red staining, sections were stained with Weigert's solution for 8 min and picrosirius red for l h. The collagen fibers were stained red with blue nuclei.

Hydroxyproline assay. Collagen content was determined by hydroxyproline levels. Dried wound tissues were hydrolyzed for 12 h at 110°C in 6 N HCl. Hydroxyproline levels were determined using chloramine T and Ehrlich's reagent. Absorbance was measured at 550 nm using a FLUOstar OPTIMA luminometer, and results were expressed as micrograms of hydroxyproline per milligram of protein.

X-gal staining. Wounded tissues in *Axin2$^{LacZ/+}$* mice were fixed with 0.4% (wt/vol) PFA in PBS for 3 h at room temperature. 20-μm wound tissue sections were fixed with 0.2% (vol/vol) glutaraldehyde in distilled water for 15 min at room temperature and stained with 1 mg/ml X-gal solution (Promega) overnight at 37°C. Cell nuclei were counterstained with nuclear fast red (Sigma-Aldrich) for 5 min at room temperature.

Quantitation of signal intensity. Immunohistochemical stainings were analyzed with TissueQuest software (TissueGnostics). Individual cells were identified based on the DAPI staining, and background threshold was specified. The intensity of specific protein above this threshold was quantified. Mean intensity was obtained from each cell, and mean values were estimated from analyses of at least three independent experimental results. ICC stainings were analyzed with NIS Elements V3.2 software (Nikon). The blue channel was referred to visualize the nuclei, and the threshold was defined for red, green, or blue channels. Mean intensity was calculated in the red and green channels separately, and mean values were estimated from analyses of three independent experimental results. Quantitative analyses of staining were performed in at least three random, representative fields.

Statistical analysis. Data are presented as means ± SD. Statistical analyses were performed using unpaired two-tailed Student's t test. Asterisks denote statistically significant differences (*, $P < 0.05$; **, $P < 0.005$; ***, $P < 0.0005$).

CXXC5 negatively regulates cutaneous wound healing | Lee et al.

REFERENCES

Akhmetshina, A., K. Palumbo, C. Dees, C. Bergmann, P. Venalis, P. Zerr, A. Horn, T. Kireva, C. Beyer, J. Zwerina, et al. 2012. Activation of canonical Wnt signalling is required for TGF-β–mediated fibrosis. *Nat. Commun.* 3:735. http://dx.doi.org/10.1038/ncomms1734

Amini Nik, S., R.P. Ebrahim, K. Van Dam, J.J. Cassiman, and S. Tejpar. 2007. TGF-β modulates β-Catenin stability and signaling in mesenchymal proliferations. *Exp. Cell Res.* 313:2887–2895. http://dx.doi.org/10.1016/j.yexcr.2007.05.024

Andersson, T., E. Södersten, J.K. Duckworth, A. Cascante, N. Fritz, P. Sacchetti, I. Cervenka, V. Bryja, and O. Hermanson. 2009. CXXC5 is a novel BMP4-regulated modulator of Wnt signaling in neural stem cells. *J. Biol. Chem.* 284:3672–3681. http://dx.doi.org/10.1074/jbc.M808119200

Barker, N. 2008. The canonical Wnt/β-catenin signalling pathway. *Methods Mol. Biol.* 468:5–15. http://dx.doi.org/10.1007/978-1-59745-249-6_1

Bergmann, C., A. Akhmetshina, C. Dees, K. Palumbo, P. Zerr, C. Beyer, J. Zwerina, O. Distler, G. Schett, and J.H. Distler. 2011. Inhibition of glycogen synthase kinase 3β induces dermal fibrosis by activation of the canonical Wnt pathway. *Ann. Rheum. Dis.* 70:2191–2198. http://dx.doi.org/10.1136/ard.2010.147140

Carthy, J.M., F.S. Garmaroudi, Z. Luo, and B.M. McManus. 2011. Wnt3a induces myofibroblast differentiation by upregulating TGF-β signaling through SMAD2 in a β-catenin–dependent manner. *PLoS ONE.* 6:e19809. http://dx.doi.org/10.1371/journal.pone.0019809

Chen, S., S. McLean, D.E. Carter, and A. Leask. 2007. The gene expression profile induced by Wnt 3a in NIH 3T3 fibroblasts. *J. Cell Commun. Signal.* 1:175–183. http://dx.doi.org/10.1007/s12079-007-0015-x

Chen, X., Y. Liu, and X. Zhang. 2012. Topical insulin application improves healing by regulating the wound inflammatory response. *Wound Repair Regen.* 20:425–434. http://dx.doi.org/10.1111/j.1524-475X.2012.00792.x

Cheon, S.S., P. Nadesan, R. Poon, and B.A. Alman. 2004. Growth factors regulate beta-catenin–mediated TCF-dependent transcriptional activation in fibroblasts during the proliferative phase of wound healing. *Exp. Cell Res.* 293:267–274. http://dx.doi.org/10.1016/j.yexcr.2003.09.029

Cheon, S., R. Poon, C. Yu, M. Khoury, R. Shenker, J. Fish, and B.A. Alman. 2005. Prolonged beta-catenin stabilization and tcf-dependent transcriptional activation in hyperplastic cutaneous wounds. *Lab. Invest.* 85:416–425. http://dx.doi.org/10.1038/labinvest.3700237

Chipev, C.C., and M. Simon. 2002. Phenotypic differences between dermal fibroblasts from different body sites determine their responses to tension and TGFβ1. *BMC Dermatol.* 2:13. http://dx.doi.org/10.1186/1471-5945-2-13

Chua, A.W., S.U. Gan, Y. Ting, Z. Fu, C.K. Lim, C. Song, K. Sabapathy, and T.T. Phan. 2011. Keloid fibroblasts are more sensitive to Wnt3a treatment in terms of elevated cellular growth and fibronectin expression. *J. Dermatol. Sci.* 64:199–209. http://dx.doi.org/10.1016/j.jdermsci.2011.09.008

Diegelmann, R.F., and M.C. Evans. 2004. Wound healing: an overview of acute, fibrotic and delayed healing. *Front. Biosci.* 9:283–289. http://dx.doi.org/10.2741/1184

Doble, B.W., and J.R. Woodgett. 2003. GSK-3: tricks of the trade for a multi-tasking kinase. *J. Cell Sci.* 116:1175–1186. http://dx.doi.org/10.1242/jcs.00384

Eisenmann, D.M. 2005. Wnt signaling. *WormBook.* June 25:1–17.

Gaur, T., L. Rich, C.J. Lengner, S. Hussain, B. Trevant, D. Ayers, J.L. Stein, P.V. Bodine, B.S. Komm, G.S. Stein, and J.B. Lian. 2006. Secreted frizzled related protein 1 regulates Wnt signaling for BMP2 induced chondrocyte differentiation. *J. Cell. Physiol.* 208:87–96. http://dx.doi.org/10.1002/jcp.20637

Gay, D., O. Kwon, Z. Zhang, M. Spata, M.V. Plikus, P.D. Holler, M. Ito, Z. Yang, E. Treffeisen, C.D. Kim, et al. 2013. Fgf9 from dermal γδ T cells induces hair follicle neogenesis after wounding. *Nat. Med.* 19:916–923. http://dx.doi.org/10.1038/nm.3181

Gould, T.D., and H.K. Manji. 2002. The Wnt signaling pathway in bipolar disorder. *Neuroscientist.* 8:497–511. http://dx.doi.org/10.1177/107385802237176

Gould, T.D., G. Chen, and H.K. Manji. 2004. In vivo evidence in the brain for lithium inhibition of glycogen synthase kinase-3. *Neuropsychopharmacology.* 29:32–38. http://dx.doi.org/10.1038/sj.npp.1300283

Guo, S., and L.A. Dipietro. 2010. Factors affecting wound healing. *J. Dent. Res.* 89:219–229. http://dx.doi.org/10.1177/0022034509359125

Hino, S., S. Kishida, T. Michiue, A. Fukui, I. Sakamoto, S. Takada, M. Asashima, and A. Kikuchi. 2001. Inhibition of the Wnt signaling pathway by Idax, a novel Dvl-binding protein. *Mol. Cell. Biol.* 21:330–342. http://dx.doi.org/10.1128/MCB.21.1.330-342.2001

Kabashima, K., J. Sakabe, R. Yoshiki, Y. Tabata, K. Kohno, and Y. Tokura. 2010. Involvement of Wnt signaling in dermal fibroblasts. *Am. J. Pathol.* 176:721–732. http://dx.doi.org/10.2353/ajpath.2010.090454

Kähäri, V.M., J. Heino, T. Vuorio, and E. Vuorio. 1988. Interferon-α and interferon-γ reduce excessive collagen synthesis and procollagen mRNA levels of scleroderma fibroblasts in culture. *Biochim. Biophys. Acta.* 968:45–50. http://dx.doi.org/10.1016/0167-4889(88)90042-0

Kasper, M., V. Jaks, A. Are, Å. Bergström, A. Schwäger, J. Svärd, S. Teglund, N. Barker, and R. Toftgård. 2011. Wounding enhances epidermal tumorigenesis by recruiting hair follicle keratinocytes. *Proc. Natl. Acad. Sci. USA.* 108:4099–4104. (published erratum appears in Proc. Natl. Acad. Sci. USA. 2012. 109:5548) http://dx.doi.org/10.1073/pnas.1014489108

Kim, H.Y., D.H. Yang, S.W. Shin, M.Y. Kim, J.H. Yoon, S. Kim, H.C. Park, D.W. Kang, D. Min, M.W. Hur, and K.Y. Choi. 2014a. CXXC5 is a transcriptional activator of Flk-1 and mediates bone morphogenic protein-induced endothelial cell differentiation and vessel formation. *FASEB J.* 28:615–626. http://dx.doi.org/10.1096/fj.13-236216

Kim, M.S., S.K. Yoon, F. Bollig, J. Kitagaki, W. Hur, N.J. Whye, Y.P. Wu, M.N. Rivera, J.Y. Park, H.S. Kim, et al. 2010a. A novel Wilms tumor 1 (WT1) target gene negatively regulates the WNT signaling pathway. *J. Biol. Chem.* 285:14585–14593. http://dx.doi.org/10.1074/jbc.M109.094334

Kim, M.S., H.J. Song, S.H. Lee, and C.K. Lee. 2014b. Comparative study of various growth factors and cytokines on type I collagen and hyaluronan production in human dermal fibroblasts. *J. Cosmet. Dermatol.* 13:44–51. http://dx.doi.org/10.1111/jocd.12073

Kim, T.H., H. Xiong, Z. Zhang, and B. Ren. 2005. β-Catenin activates the growth factor endothelin-1 in colon cancer cells. *Oncogene.* 24:597–604. http://dx.doi.org/10.1038/sj.onc.1208237

Kim, Y.S., D.H. Lew, K.C. Tark, D.K. Rah, and J.P. Hong. 2010b. Effect of recombinant human epidermal growth factor against cutaneous scar formation in murine full-thickness wound healing. *J. Korean Med. Sci.* 25:589–596. http://dx.doi.org/10.3346/jkms.2010.25.4.589

Krieg, T., J.S. Perlish, R. Fleischmajer, and O. Braun-Falco. 1985. Collagen synthesis in scleroderma: selection of fibroblast populations during subcultures. *Arch. Dermatol. Res.* 277:373–376. http://dx.doi.org/10.1007/BF00509236

Labus, M.B., C.M. Stirk, W.D. Thompson, and W.T. Melvin. 1998. Expression of Wnt genes in early wound healing. *Wound Repair Regen.* 6:58–64. http://dx.doi.org/10.1046/j.1524-475X.1998.60109.x

Ladin, D.A., W.L. Garner, and D.J. Smith Jr. 1995. Excessive scarring as a consequence of healing. *Wound Repair Regen.* 3:6–14. http://dx.doi.org/10.1046/j.1524-475X.1995.30106.x

Lan, Y., H. Li, Y.Y. Chen, Y.W. Zhang, N. Liu, Q. Zhang, and Q. Wu. 2014. Essential oil from *Zanthoxylum bungeanum* Maxim. and its main components used as transdermal penetration enhancers: a comparative study. *J. Zhejiang Univ. Sci. B.* 15:940–952. http://dx.doi.org/10.1631/jzus.B1400158

Lee, S.H., M. Zahoor, J.K. Hwang, S. Min, and K.Y. Choi. 2012. Valproic acid induces cutaneous wound healing in vivo and enhances keratinocyte motility. *PLoS ONE.* 7:e48791. http://dx.doi.org/10.1371/journal.pone.0048791

Li, C.H., and S. Amar. 2006. Role of secreted frizzled-related protein 1 (SFRP1) in wound healing. *J. Dent. Res.* 85:374–378. http://dx.doi.org/10.1177/154405910608500418

Liao, D.J., A. Thakur, J. Wu, H. Biliran, and F.H. Sarkar. 2007. Perspectives on c-Myc, Cyclin D1, and their interaction in cancer formation, progression, and response to chemotherapy. *Crit. Rev. Oncog.* 13:93–158. http://dx.doi.org/10.1615/CritRevOncog.v13.i2.10

London, T.B., H.J. Lee, Y. Shao, and J. Zheng. 2004. Interaction between the internal motif KTXXXI of Idax and mDvl PDZ domain. *Biochem. Biophys. Res. Commun.* 322:326–332. http://dx.doi.org/10.1016/j.bbrc.2004.07.113

Matsushita, M., and H. Matsui. 2005. Protein transduction technology. *J. Mol. Med.* 83:324–328. http://dx.doi.org/10.1007/s00109-004-0633-1

Niida, A., T. Hiroko, M. Kasai, Y. Furukawa, Y. Nakamura, Y. Suzuki, S. Sugano, and T. Akiyama. 2004. DKK1, a negative regulator of Wnt signaling, is a target of the β-catenin/TCF pathway. *Oncogene.* 23:8520–8526. http://dx.doi.org/10.1038/sj.onc.1207892

Özyazgan, I., and O. Kontaş. 2004. Previous injuries or scars as risk factors for the development of basal cell carcinoma. *Scand. J. Plast. Reconstr. Surg. Hand Surg.* 38:11–15. http://dx.doi.org/10.1080/02844310310005883

Rizvi, M.A., L. Katwa, D.P. Spadone, and P.R. Myers. 1996. The effects of endothelin-1 on collagen type I and type III synthesis in cultured porcine coronary artery vascular smooth muscle cells. *J. Mol. Cell. Cardiol.* 28:243–252. http://dx.doi.org/10.1006/jmcc.1996.0023

Sato, M. 2006. Upregulation of the Wnt/β-catenin pathway induced by transforming growth factor-β in hypertrophic scars and keloids. *Acta Derm. Venereol.* 86:300–307. http://dx.doi.org/10.2340/00015555-0101

Singer, A.J., and R.A. Clark. 1999. Cutaneous wound healing. *N. Engl. J. Med.* 341:738–746. http://dx.doi.org/10.1056/NEJM199909023411006

Tang, J., H. Liu, C. Gao, L. Mu, S. Yang, M. Rong, Z. Zhang, J. Liu, Q. Ding, and R. Lai. 2014. A small peptide with potential ability to promote wound healing. *PLoS ONE.* 9:e92082. http://dx.doi.org/10.1371/journal.pone.0092082

Wei, J., D. Melichian, K. Komura, M. Hinchcliff, A.P. Lam, R. Lafyatis, C.J. Gottardi, O.A. MacDougald, and J. Varga. 2011. Canonical Wnt signaling induces skin fibrosis and subcutaneous lipoatrophy: a novel mouse model for scleroderma? *Arthritis Rheum.* 63:1707–1717. http://dx.doi.org/10.1002/art.30312

Whyte, J.L., A.A. Smith, B. Liu, W.R. Manzano, N.D. Evans, G.R. Dhamdhere, M.Y. Fang, H.Y. Chang, A.E. Oro, and J.A. Helms. 2013. Augmenting endogenous Wnt signaling improves skin wound healing. *PLoS ONE.* 8:e76883. http://dx.doi.org/10.1371/journal.pone.0076883

Yamaguchi, Y., and K. Yoshikawa. 2001. Cutaneous wound healing: an update. *J. Dermatol.* 28:521–534. http://dx.doi.org/10.1111/j.1346-8138.2001.tb00025.x

Zhang, D.L., L.J. Gu, L. Liu, C.Y. Wang, B.S. Sun, Z. Li, and C.K. Sung. 2009a. Effect of Wnt signaling pathway on wound healing. *Biochem. Biophys. Res. Commun.* 378:149–151. http://dx.doi.org/10.1016/j.bbrc.2008.11.011

Zhang, M., R. Wang, Y. Wang, F. Diao, F. Lu, D. Gao, D. Chen, Z. Zhai, and H. Shu. 2009b. The CXXC finger 5 protein is required for DNA damage-induced p53 activation. *Sci. China C Life Sci.* 52:528–538. http://dx.doi.org/10.1007/s11427-009-0083-7

Zhang, S., W. Wang, Y. Peng, Q. Gu, J. Luo, J. Zhou, J. Wu, Y. Hou, and J. Cao. 2014. Amelioration of radiation-induced skin injury by HIV-TAT-mediated protein transduction of RP-1 from Rana pleurade. *Int. J. Med. Sci.* 11:44–51. http://dx.doi.org/10.7150/ijms.7463